The University of Hull

CYCLIC DIPEPTIDES AND THEIR SELF-ASSEMBLING PROPERTIES

being a Thesis submitted for the degree of
MSc (by Research) Chemistry
at the University of Hull

by

Jacob Balangtaa
BSc(Hons) (University of Hull)

May 2017

Risk Assessment

All experiments were carried out in accordance with the University of Hull's Health and Safety guidelines. A full COSHH and risk assessment was carried out for each new experiment, signed by the undertaking student, supervisor; Dr. Michael Reithofer, and the departmental safety officer (Dr. Tom McCreedy) before any practical work started. The COSHH forms carry the reference numbers JB01, JB02, JB03 and JB04.

Acknowledgment

I would like to thank Dr. Michael Reithofer and co-supervisor Dr. Jia Min Chin for their supervision and also the University of Hull scholarship (D. E. Stromberg).

I also wish to express my gratitude to Zahraa Al-Mashaykhi, Akinola Taiwo Oluwaseun and Dr. Chris Welch for their help in general, Dr. Kevin Welham (mass spectrometry), Dr. Robert Lewis (NMR), Prof. Bernard Binks (SEM) and Dr. Jean-Sebastien Bouillard (Photoluminescence).

Abstract

Over recent years, cyclic dipeptides, or 2,5-diketopiperazines, have found numerous applications in nanotechnology, such as biological drug delivery. Reasons for this include their ease of synthesis and numerous intrinsic properties. One such property is self-assembly, wherein the cyclic dipeptide can undergo molecular reorganisation in certain conditions, and exhibit a novel structure. This reorganisation can be achieved in different ways; the results often vary depending on the original conditions.

A popular method of synthesising linear dipeptides is through solid phase peptide synthesis, which has numerous advantages compared to the older solution phase method. In this project, Fmoc solid phase peptide synthesis (SPPS) was employed to synthesise four different linear dipeptides, and their cyclisation and subsequent self-assembly probed in different solvents. The dipeptides used were chosen based on their varying aromatic side-chains, whilst solvents of varying polarities were utilised.

Linear dipeptides were added to the solvents, and it was seen that many of them were insoluble in certain solvents. The ones that did dissolve were heated and tested for unconventional cyclisation. Cyclic dipeptide analogues from the initial sequences *H*-FF-*OH*, *H*-HH-*OH*, *H*-HF-*OH* and *H*-HY-*OH* were confirmed and found to have a self-assembled structure in each solvent they originated from. Cyclic FF (cFF, cyclised from linear *H*-FF-*OH*), self-assembled in the most number of solvents, and produced a similar structure in each of them. In addition, cyclic FF that self-assembled in 1,4-dioxane was found to have blue-luminescent properties. It was also observed that the amount of self-assembly was affected by the temperature each solvent containing the peptide was subjected to. cHH self-assembled in only one solvent, n-PrOH, whereas cHF and cHY both self-assembled in i-PrOH and THF. Self-assembled cFF was observed to be made of rod-like strands whereas self-assembled cHH appeared to be composed of a hierarchal structure consisting of needle-like components in an “urchin-like” sphere. Self-assembled cHF and cHY had a mixture of structures derived from those seen in cFF and cHH, with a notable flower-like entity seen for cHY self-assembled in THF.

List of Abbreviations

AA	amino acid
ACN	acetonitrile
AFM	atomic force microscopy
Boc	tert-butyloxycarbonyl
DCC	1,3-dicyclohexylcarbodiimide
DCM	dichloromethane
DIC	N,N'-Diisopropylcarbodiimide
DIPEA	N,N-Diisopropylethylamine
DMAP	4-(Dimethylamino)pyridine
DMF	dimethylformamide
Et_2O	diethyl ether
EtOH	ethanol
FESEM	field emission scanning electron microscopy
Fmoc	9-fluorenylmethoxycarbonyl
HF	hydrofluoric acid
HFIP	hexafluoro-2-propanol
HOBt	1-hydroxybenzotriazole
i-PrOH	propan-2-ol
MeOH	methanol
NMR	Nuclear Magnetic Resonance
n-PrOH	propan-1-ol
SPPS	solid phase peptide synthesis

TBTU	*N*-[(1*H*-benzotriazol-1-yl)(dimethylamino)methylene]-*N*-methylmethanaminium tetrafluoroborate N-oxide
tBu	tert-butyl
TEM	transmission electron microscopy
TFA	trifluoroacetic acid
THF	tetrahydrofuran
TIS	triisopropylsilane
trt	trityl
UV	ultraviolet

List of Figures

List of Tables

Table of Contents

Chapter One

Introduction

Chapter 1. Introduction

1.1 Overview

In the field of nanotechnology, peptides have been under much investigation.[1] This is because of their potential. For example, taking into account the activities of biological proteins, such molecules are able to selectively bind to other molecules and function as smart materials. An example of a peptide is diphenylalanine (*H*-FF-*OH*), a core constituent of the Alzheimer's β-amyloid polypeptide.[2] Synthetic peptides are not difficult to be made chemically,[3] and they can be used as templates to construct sensors and nanodevices.

"Self-assembly" is a term in nanotechnology used to describe the spontaneous ordering of individual units into bigger aggregates. These aggregates are often of interest because of their unique properties. Among many other materials, self-assembly can result in the formation of regular molecular crystals,[4] semicrystalline polymers[5] and gels.[6]

When subjected to certain conditions, peptides can undergo self-assembly. The underlying theory is that this process is caused by non-covalent supramolecular interactions such as hydrophobic binding, aromatic-aromatic interactions, hydrogen-bonding, van der Waals and electrostatic forces.[7,8] Cyclic peptides, formed from ordinarily linear peptides, have also demonstrated the ability to self-assemble.

The central terms underlying this thesis are **peptides**, **peptide cyclisation** and **self-assembly**. An employed method of experimentation, i.e. the heating of predissolved peptides in solvents, will address two main problems; "What is the role of heating solvents in terms of *peptide cyclisation*?" and, "Did the *cyclised peptides* subsequently undergo *self-assembly* in the same solvents they were heated in?" In this chapter, **1.2** is the relevant literature review for peptide self-assembly. **1.3** examines self-assembly fundamentals. **1.4** goes into further detail about cyclic peptides, with some examples of their applications. **1.5** is the development of two main synthetic peptide routes. Finally, **1.6** covers what this project aims to do in comparison to the literature.

1.2 Research in context

The main theme of this project is organic nanotechnology (with an emphasis on aromatic peptides), which is relatively new compared to other known nanotechnology such as carbon nanotubes.[9] Some of the earliest research in this field dates back to 1993, where Ghadiri and his co-workers first described hollow peptide nanotubes based on cyclic polypeptides.[10] When these peptides protonated, they crystallised into nanotubes with an internal diameter of 7-8 Å. Zhang and his group (2003) were among the first to show that peptides efficiently self-assembled in an aqueous solution.[11] They demonstrated that ionic self-complementary peptides could form hydrogels (Fig. 1).

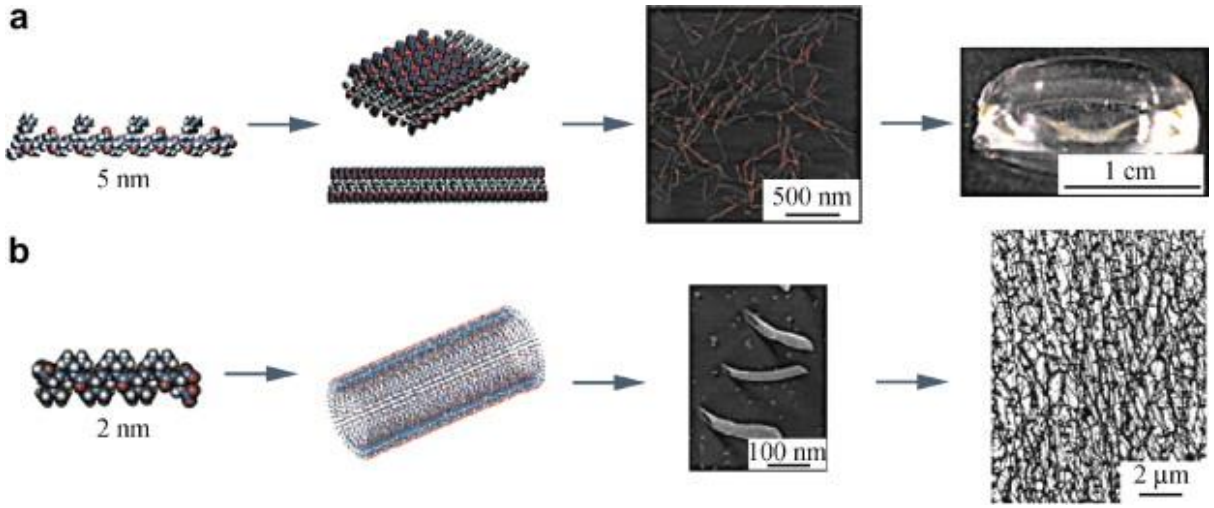

Figure 1. Peptide research from Zhang et al. a) are ionic self-complementary peptides forming hydrogels; b) are surfactant-like peptides.[11]

The following are contemporary studies concerning the amino acids used in this project, namely phenylalanine, tyrosine and histidine.

Phenylalanine

In recent years, phenylalanine-based nanotechnology has been researched extensively. Diphenylalanine peptides are among the smallest peptide sequences to have reported self-assembly.[12] The dipeptide L-Phe-L-Phe (*H*-FF-*OH*) has been reported to form organogels in chloroform and toluene.[13] In this study, Yan et al. (2008) determined the self-assembled gels to be made of L-Phe-L-Phe nanofibrils, and proposed that π-π stacking led to peptide β-sheets which resulted in the nanofibrils (Fig. 2).

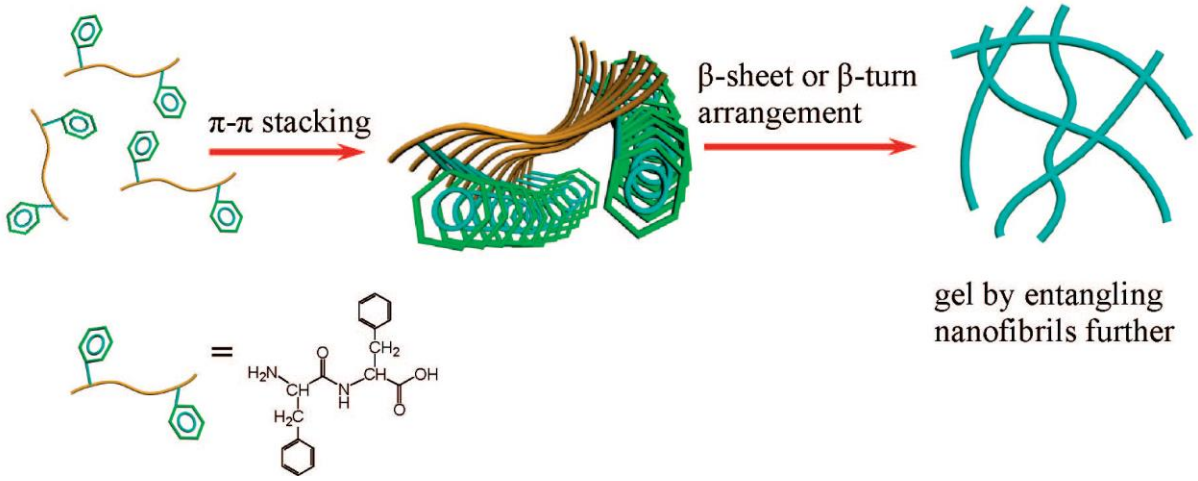

Figure 2. A proposed model of the self-assembly process, where aromatic stacking eventually leads to nanofibril formation.[13]

The group of Adler-Abramovich and Gazit have also widely covered phenylalanine-based self-assembly.[3] One of their novel research outputs in the area (2009) demonstrated that linear *H*-FF-*OH* self-assembled onto a substrate as cyclic FF via vapour-phase deposition.[14] The mechanism they proposed for this was that on heating to 220 °C, linear *H*-FF-*OH* cyclised and subsequently deposited onto the substrate as vertically aligned nanotubes (Fig. 3).

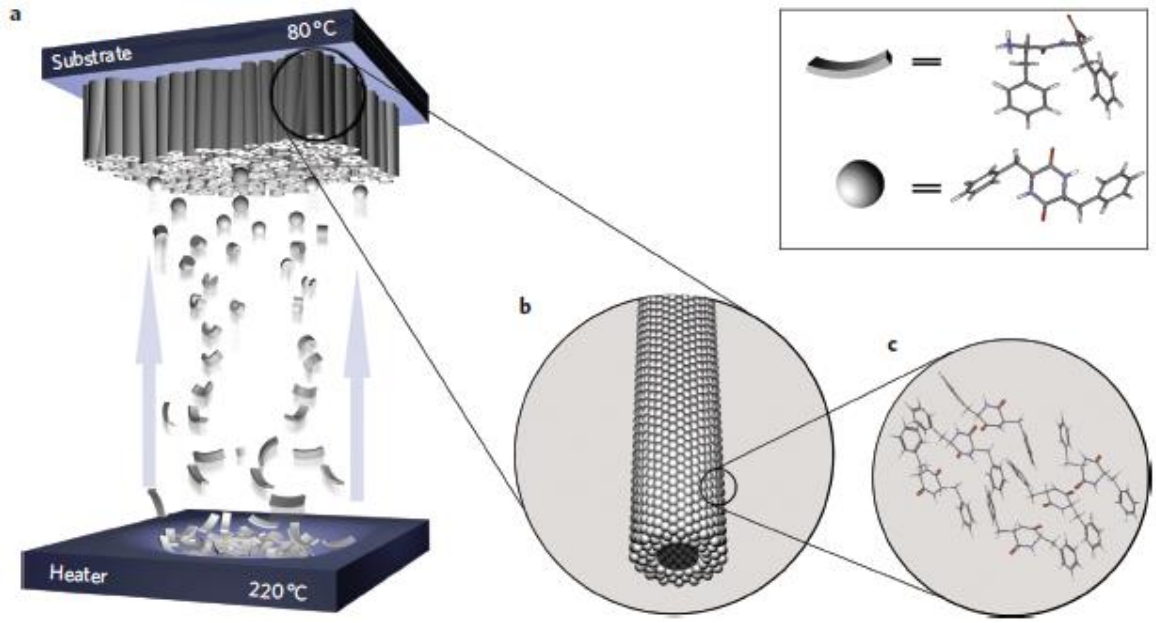

Figure 3. The proposed self-assembly mechanism of vertically aligned cyclic FF nanotubes. a) The vapour deposition process, where linear H-FF-OH, when heated at 220 °C, cyclises and deposits on the substrate at 80 °C. b) Depiction of a single nanotube comprising of cyclic FF. c) Scheme of six cFF peptides stacked together which gives directionality of the overall nanotubes.[14]

Tyrosine

Tyrosine (Y) has also been shown to display self-assembling properties. In 2015, Ménard-Moyon and her co-workers demonstrated that L-tyrosine, when added to water in different concentrations, produced nanoribbons.[15] Short peptides containing tyrosine have been reported to have self-assembling properties. Min et al. (2016) synthesised the peptide sequence YYAYY, which, when irradiated with UV in a pH 10 buffer and followed by dialysis, formed hollow nanocapsules.[16]

Histidine

Due to the nature of imidazole on histidine (H), this amino acid has the ability to bind to metals such as copper (Fig. 4).[17]

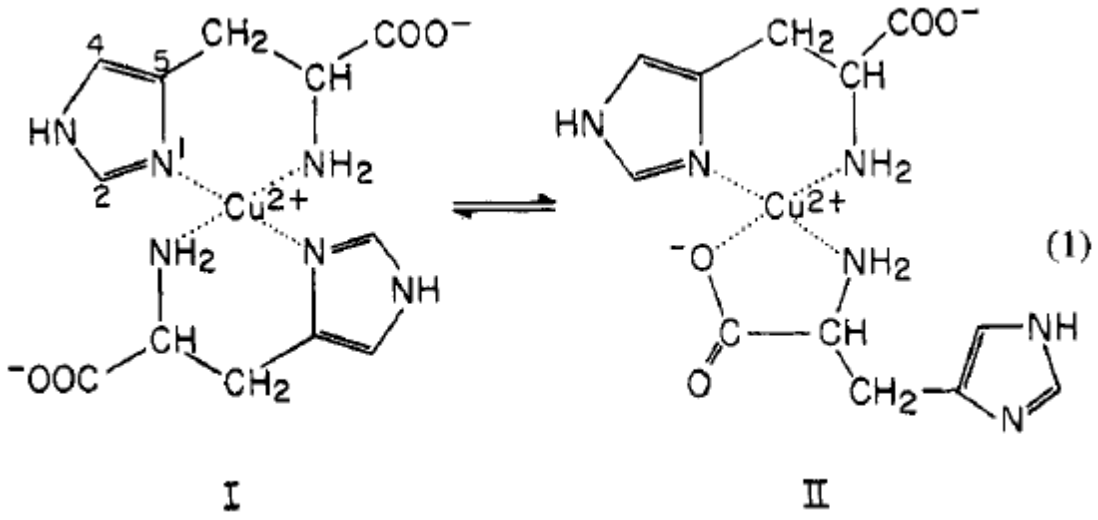

Figure 4. The Structure of the Copper (II) -L-Histidine 1:2 Complex in D_2O Solution; structures I and II are the different arrangements of the complex in equilibrium.[17]

This property has been exploited in many metal-based studies, for example the self-assembly of histidine-containing peptides onto gold nanoparticles and quantum dots, reported by Mattoussi and his group in 2013.[18] They also explored the metal-histidine coordination kinetics of the two proteins used, a His-appended maltose binding protein (MBP-His) and a fluorescent His-terminated mCherry protein.

Cyclic hetero-dipeptides

This concerns work relating to the cyclic hetero-dipeptide aspect in this project (where cyclic homo-dipeptides are for example cFF, and hetero-dipeptides are cHF, etc.). Jeziorna and her co-researchers (2015) synthesised two dipeptides, cyclo(L-Tyr-L-Ala) and cyclo(L-Tyr-D-

Ala), via the traditional chemical method, with the purpose of studying the effect the different diastereomers of Ala had on the self-organisation of the peptides in solution and their heating in the solid state.[19] In their study, differential scanning calorimetry, SEM, powder X-ray diffraction, solid state NMR, IR and electronic circular dichroism were used, which illustrates the numerous experimental techniques that can be used to analyse the self-assembly and subsequent crystallisation of cyclic peptides. As seen in Figs. 5 and 6, they showed that the different diastereomers of Ala in fact had an effect on the morphology of the self-assembled peptides.

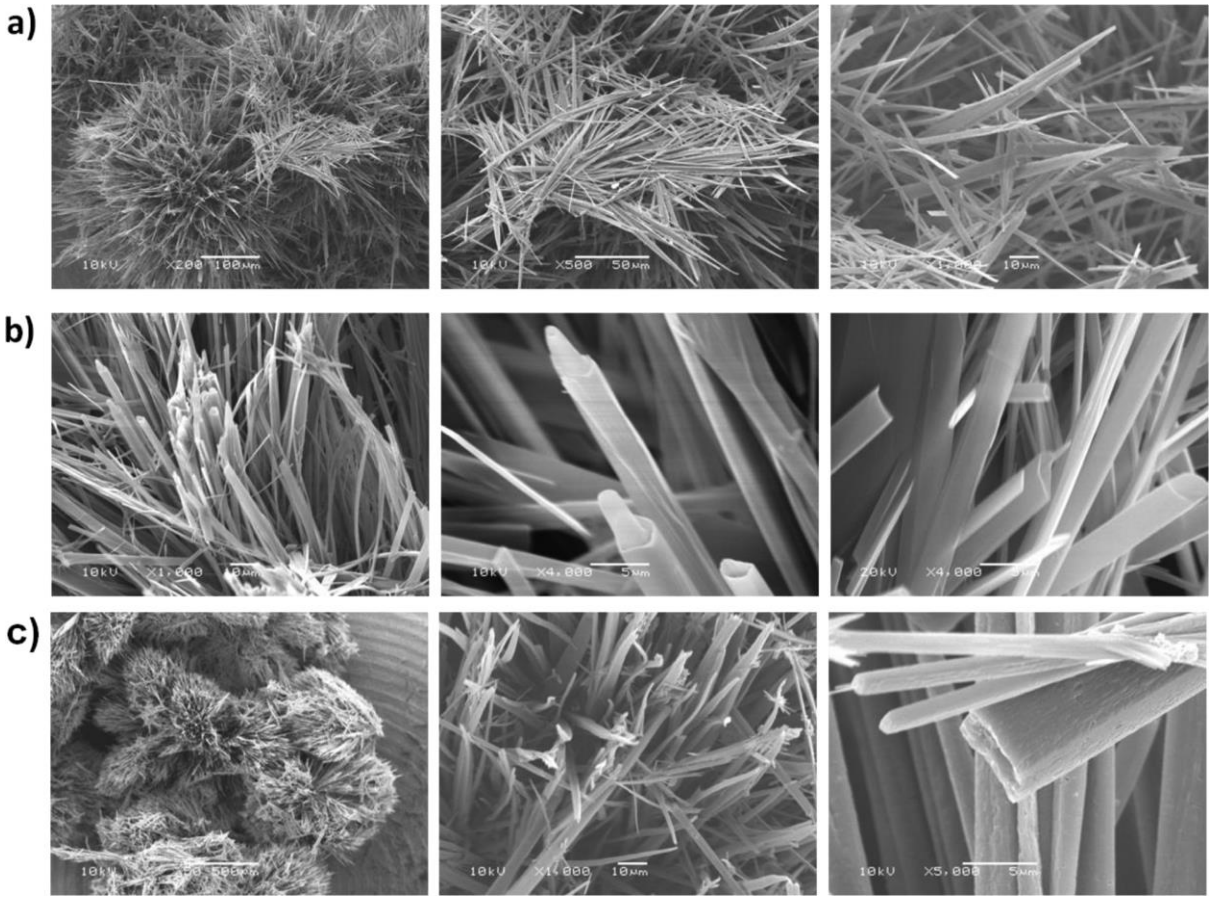

*Figure 5. SEM Images of cyclo(L-Tyr-L-Ala), or cYA **1**. a) is the dipeptide after crystallisation in a 1:1 MeOH/H_2O solution, b) is the thermal treatment of H_2Tyr(L)AlaOH in solid state, c) is the dipeptide after heating at 160 °C.*[19]

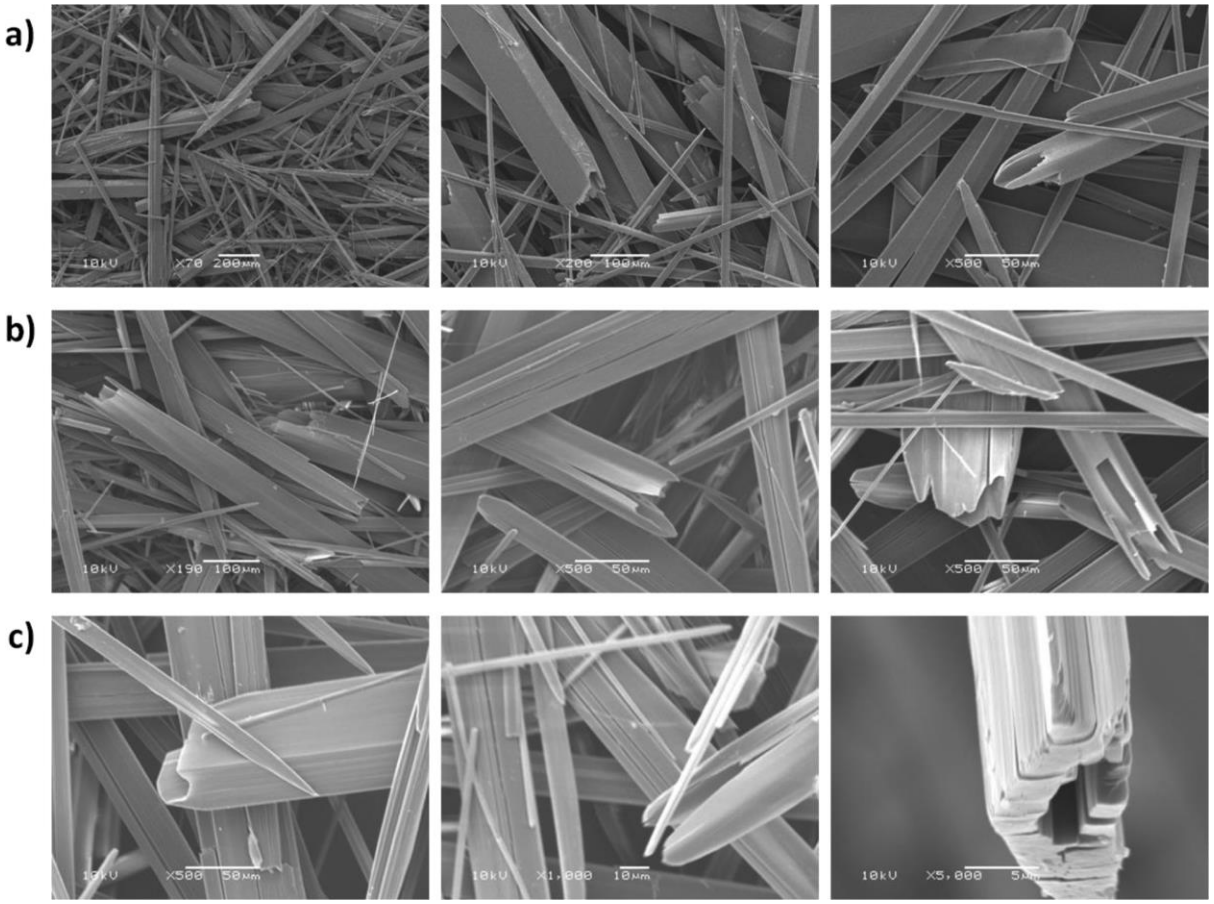

*Figure 6. SEM Images of cyclo(L-Tyr-D-Ala), or cYA **2**. a) is the dipeptide after crystallisation in a 1:1 MeOH/H_2O solution, b) is the dipeptide after heating at 130 °C and c) is the dipeptide after heating at 160 °C.*[19]

In 2013, Nachtsheim and his group synthesised phenylalanine-containing cyclic dipeptides through conventional synthesis, heated an aqueous suspension of each dipeptide (4 wt% dipeptide) until dissolution, and cooled each solution to room temperature.[20] Their results showed that all the cyclic dipeptides tested formed hydrogels (Fig. 7).

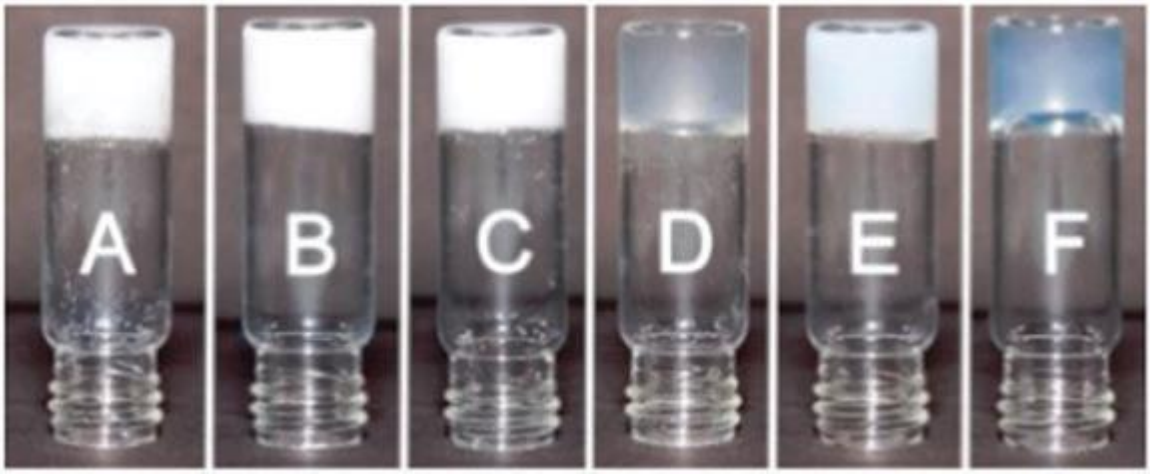

Figure 7. Photos of different cyclic dipeptides after they were heated in aqueous solution (4 wt%) and cooled to room temperature. All of them formed hydrogels. (A) cyclo(L-Phe-Gly) (B) Cyclo(L-Phe-L-Ser) (C) Cyclo(L-Phe-L-Cys) (D) Cyclo(L-Phe-L-Glu) in phosphate buffer/ pH 6.0. (E) Cyclo(L-Phe-L-His) (F) Cyclo(L-Phe-L-Lys).[20]

The self-assembly, with regards to crystallisation/gelation properties for three cyclic dipeptide sequences in this project (cHH, cHF and cHY), has not been investigated to the extent seen for cFF so far.

1.3 Self-assembly

The broader termed "supramolecular chemistry" is the chemistry of molecular assemblies where individual structural units combine to form a multicomponent system.[21] The units themselves are normally held by weaker non-covalent interactions, although there are supramolecular systems where covalent metal-donor bonds bind together organic components.[22] Self-assembly is a process in which individual components form ordered aggregates spontaneously, via localised and specific interactions between the components.[23] That is, without human intervention. A key aspect to this definition is the spontaneous ordering of the aggregates. One important note is that the molecular forces here are the same ones found in Nature to bind molecular assemblies, and much of the work in supramolecular chemistry deals with mimicking these systems.[24]

Self-assembled structures

As mentioned in the overview (**1.1**), self-assembly can give rise to crystalline structures and gels. The distinction between self-assembly and crystallisation is that although self-assembly leads to crystallisation, it focuses on matter designed *rationally* at < 100 nm scales, and that the components have to assemble themselves spontaneously in order to realise this.[25] The

general term *gel* is used to define solid-like substances where a liquid is the dispersed phase and a solid is the dispersion medium/continuous phase. Physical gelation can occur when self-assembled fibrous networks (formed by intermolecular interactions), caused by *gelator* molecules, entrap a solvent within those networks.[26] Examples of gels formed in such a manner are the hydrogels (liquid is water) and organogels (organic liquid) alluded to in **1.2**, and xerogels (liquid removed by evaporation).

Experimental techniques such as SEM and optical microscopy can be used to view the overall self-assembled structure, whereas differential scanning calorimetry, powder X-ray diffraction, solid state NMR and electronic circular dichroism can be used to determine the crystallinity of the structure. The first two techniques will be employed in this project.

The interactions governing self-assembly can be subdivided into the following:

Electrostatic Interactions

These interactions are based on molecular charges. They can be attractive between ions or molecules with opposite charges. Similarly, they can be repulsive between ions or molecules of same charges. Pure electrostatic interactions are not directional in nature. The strength of these interactions are also dependent on the medium that the molecules are present in. For example, the interactions between opposite unit charges may be much weaker in polar media compared to the interactions between these same units (with opposite charges) in a vacuum.

Hydrogen Bonding

Considered as a specific type of electrostatic interaction, this can be described an attractive interaction between a proton donor and a proton acceptor. Hydrogen bonds are also directional in nature, allowing them to be functionally used in supramolecular chemistry.

Van der Waals Interactions

These interactions consist of intermolecular dispersive and inductive forces (Keesom force, Debye force and London dispersion forces). They are caused by the interactions of neighbouring electron clouds (between atoms or molecules), and are long range in the sense that they occur between molecules at distances larger than the sum of their electron clouds.[21] Van der Waals forces are non-directional.

π-π Interactions

The long-held belief was that these were directional forces arising from the attractive interactions between aromatic-surface π electron clouds, allowing for aromatic groups to "stack" on top of each other.[27] However, it has recently been proposed that such a definition does not completely reflect the current experimental evidence.[28] It has been argued that the more accurately termed "aromatic-aromatic" interactions are also largely due to electrostatic interactions between neighbouring electron-rich and electron-deficient aromatics, as well as energetically dominant solvation/desolvation effects, such as the hydrophobic effect in polar solvents.[29] As an example in supramolecular chemistry, these interactions have been exploited in the host-guest self-assembly of pseudorotaxane systems[30,31] In peptide chemistry, these interactions can be found on peptides containing the aromatic amino acids phenylalanine, histidine, tyrosine and tryptophan.[32]

Hydrophobic Binding

These take place among molecules in a solution. These interactions have not been completely understood, and different views have emerged over time. The classical view holds that there is a tendency for solvent molecules to seek their most stable hydrogen-bonded environment.[21] In solution, water molecules form enhanced hydrogen bonding around a hydrophobic component, leading to clusters or "icebergs" being observed.[33] The dynamic view claims that hydrogen bonding and water structure remains unchanged; rather, the hydrophobic solute hampers the jump mechanism of the water molecules' rotational relaxation, thus slowing the dynamics of those water molecules.[34] Another recent view suggests that the van der Waals attraction between the hydrophobic solute's carbon and the water's oxygen result in an increased ordering of water in the hydration shell of the hydrophobic component.[35] Hydrophobic binding has been found to contribute to the stability of a large protein, the Borrelia burgdorferi protein (VlsE),[36] when it folds in urea[37].

The table below shows the relative bonds strengths and lengths of these non-covalent interactions. Although each of these interactions is individually weak compared to a typical covalent bond (around 100 – 400 kJ mol^{-1}), a combination of all these forces is enough to hold a self-assembled structure in place.

Interaction	Typical Bond strength/kJ mol^{-1}	Typical Bond length/Å
Electrostatic	50 - 200	~ 2.5
Hydrogen bonding	4 - 60	2.5 – 3.0
Van der Waals	0.5 - 3	3 - 4
π-π Interactions	0 - 50	~ 3.8
Hydrophobic binding	< 40	varies

Table 1 Non-covalent interactions and their relative bond strengths and lengths.[38- 40]

1.4 Peptides

The naming convention of a peptide is to start with the N-terminal amino acid and end at the C-terminal amino acid, from left to right.[41] For example, for a peptide which consists of alanine, aspartic acid and glutamine, where the N-terminal is on alanine and the C-terminal is on glutamine, the name would be *H*-ADQ-*OH*.

Dipeptides consist of the minimum number of amino acids needed to make a peptide, i.e. two. Dipeptides and other short peptides such as tripeptides are common subjects of modern research, given their accessibility, relatively low cost and ability to form new materials such as hydrogels.[42]

Cyclic peptides

When a linear peptide forms a circular ring structure via a covalent bond between an intrinsic N-terminus and C-terminus group, the new entity is known as a cyclic peptide.[43] Cyclic peptides are interesting topics of research because they show greater stability compared to conventional linear peptides,[44] and as such, show promise as drug scaffolds.[45] Due to them not having charges stemming from carboxylic and amine terminal groups, they can be very permeable in the digestive tract and easily absorbable.[46]

When dipeptides cyclise, they form what are known as 2,5-diketopiperazines, and these are the smallest cyclic peptides.[47] They can be found in natural products from sources such as bacteria and fungi.[48] By way of an example, the structural difference between a cyclic dipeptide and another cyclic derivative is shown in Figs. 8 (2,5-diketopiperazine) and 9 (cyclic tetrapeptide).

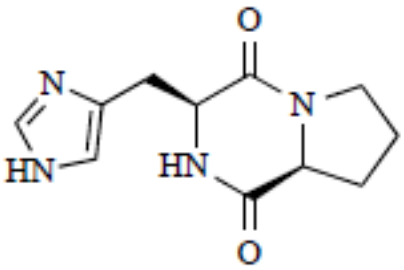

Figure 8. Cyclo(His-Pro), a biologically active peptide produced by the enzymatic cleavage of the hypothalamic Thyrotropin-releasing hormone.[49]

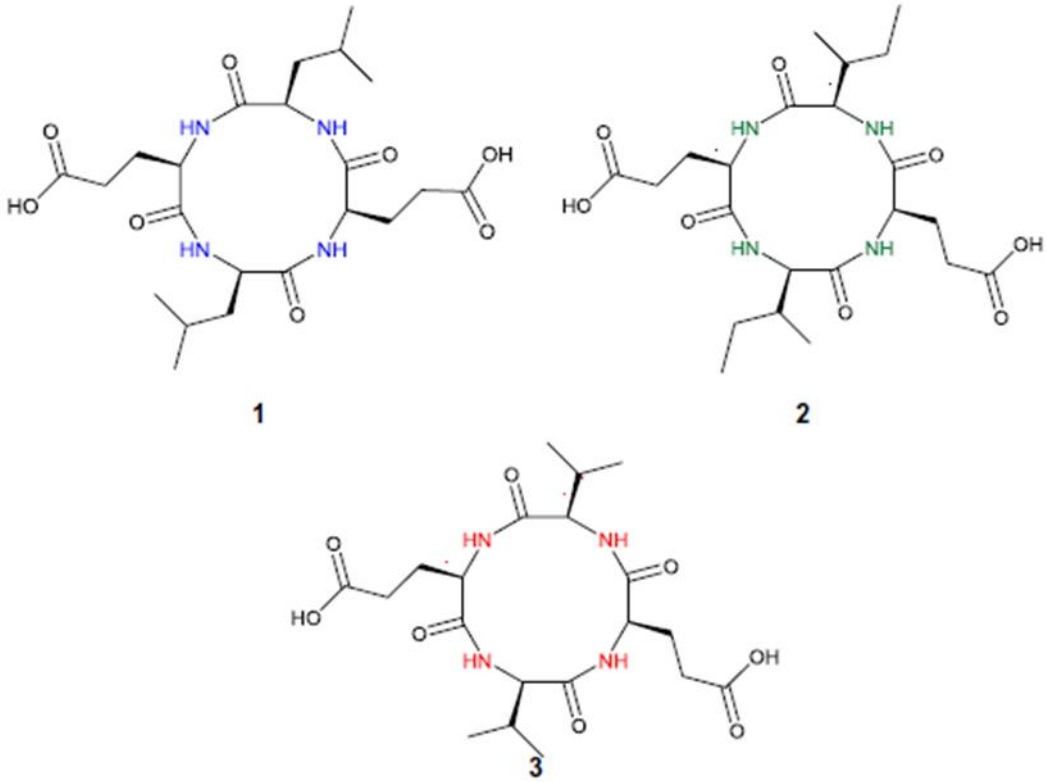

Figure 9. The cyclotetrapeptides [1: cyclo-(L-Leu-L-Glu-L-Leu-L-Glu)] [2: cyclo-(L-Ile-L-Glu-L-Ile-L-Glu)] [3: cyclo-(L-Val-L-Glu-L-Val-L-Glu)] isolated from Streptomyces sp. 447, obtained from endophytic actinobacteria.[50]

Cyclic dipeptides have found use in the field of biology, in areas such as drug delivery. For example, in one study, Diclofenac, a nonsteroidal anti-inflammatory drug, was conjugated to a novel cyclic phenylalanyl-N-methyl-naphthalenylalanine-derived shuttle and to a cell penetrating peptide TAT (GRKKRRQRRRPQ).[51] The resulting compound strengthened the

delivery of the drug through human epidermis, with a significant contribution from the cyclic dipeptide.

As evidenced in **1.2**, cyclic dipeptides can also function as low molecular weight (LMW) gelators. Cyclo(Gly-L-Lys) derivatives can form organogels in toluene and hydrogels in water, and a derivative of this cyclic compound self-assembles into a microporous hierarchal structure with excimer emission properties in chloroform.[52]

The conventional route to achieve peptide cyclisation is standard organic synthesis, i.e. by way of many chemical reactions and reagents.[53] With that said, amides, or more specifically cyclic peptides, are not usually formed by the sole heating of amine and carboxylic acid precursors. For the case of dipeptides, recent developments have shown that when they are heated *alone*, they can lose water and cyclise.[54-57] Thus, this unusual method of cyclisation via simple heating is an interesting rarity. It is suspected that the driving force behind this mechanism is the formation of the more thermodynamically favoured cyclised product, compared to the starting precyclised unit.[58]

This method of cyclisation has been demonstrated as the vertically aligned cFF nanotubes (**1.2)**, wherein the starting linear peptide was heated to 220 °C. The unique experimentation route for this project follows the spirit of this cyclisation mechanism. Simple heating will be utilised, however, it is unique in the sense that **heating dipeptides in solvents only** as a means of achieving cyclisation has so far not been attempted.

Similar to standard procedures in organic chemistry, the difference between a cyclic peptide and linear peptide can be seen in molecular characterisation using techniques such as MS and NMR. This is done by comparing the molecular structure of each, and noticing the difference in peaks between the spectra, which are due to distinct molecular arrangements between the cyclic and linear peptide. This type of characterisation will be utilised in this project.

The relationship between cyclisation and self-assembly is that products formed from covalent peptide cyclisation can take part in self-assembly, depending on the conditions subjected to them. In other words, cyclic peptides are a distinct class of materials, like linear peptides, that exhibit self-assembling properties.

1.5 Peptide Synthesis

Since amino acids have two or three different functional groups which could react to give unwanted by-products, those groups need to be protected beforehand to obtain the desired peptide. There are two main routes to synthesise peptides.

1.5.1. Solution Phase

In 1901, the first published synthetic dipeptide was made by Emil Fischer.[59] Here, a glycine diketopiperazine was hydrolysed in the solution phase to give glycylglycine.[60] The conventional solution phase method involves the step-by-step coupling of individual amino acids with other reagents in solution.[3] Each amino acid is eventually involved in a condensation reaction with another, and this process is repeated until the desired peptide is obtained.[61] An advantage of this method is that at any stage, the intermediates could be isolated and by-products removed, thus improving the yield of the final product.[62] The disadvantage is that the purification steps can be time-consuming, a lot of reagents and solvents need to be used, and a lot of waste material is also generated.[63] Up to date, there have been many variations of the conventional solution phase synthesis.[64] One recent method involves group-assisted purification chemistry where peptides can be synthesised efficiently without the need for chromatography or recrystallisation.[63] However, before these newer alternative routes emerged, another standard method of peptide synthesis was developed.

1.5.2. Solid Phase

In 1963, Robert Bruce Merrifield invented SPPS to improve peptide synthesis efficiency.[65] Amino acids are consecutively coupled to each other in a step-by-step manner. Synthesis starts at the C-terminal and ends at the N-terminal of the peptide. An insoluble polymer support such as polystyrene acted as a carboxyl-protecting group for the C-terminal amino acid start of the peptide, which was already N-protected. Functionalized linker groups were attached to the polystyrene support, and these two collectively made up a resin. The initial resins were chloromethylated polystyrene divinylbenzene particles (PS-DVB). After the N-protecting group was removed, the next amino acid was coupled with the help of a coupling agent such as DCC. Stepwise, more amino acids as desired were coupled to the preceding ones, and all this was done on the polymer support. All the solvents were organic, and this took place at room temperature. Finally, the peptide was deprotected and cleaved from the resin by treatment with an acid such as HF and chemical scavengers.[66] Some advantages of this technique, over

solution phase synthesis, include: the reaction proceeds by an excess of reactants and reagents; the final peptide is obtained in a single cleavage step (side chains also deprotected at this stage); and any by-products can be removed from the growing peptide since it is attached to the resin.[67- 69] Over time, many improvements were made to the original design such as the use of a polar polydimethyl acrylamide resin by Sheppard.[70]

In the early designs of SPPS, amino acid protecting groups such as Boc were used. The problem with this was that there was an incomplete differentiation in reaction conditions for the protecting group cleavage.[71] In addition, cleaving Boc groups repetitively by TFA may damage long peptide synthesis, and the side chains in histidine, tryptophan, tyrosine and methionine may experience trifluoro acetylation with the TFA.[72] Sheppard et al. (1989) investigated different base-labile N-terminal protecting groups for application in SPPS, [73] and found the Fmoc group proposed by Carpino in 1972[74] (which was not favourable for solution phase synthesis since organic base cleavage resulted in reactive dibenzofulvene that could take part in addition/polymerization reactions[73]) to be well suited. In addition to overcoming the problems with Boc mentioned earlier, other advantages of this approach include: milder conditions are required where deprotection can be done by a non-hydrolytic base like piperidine and final cleavage by TFA; it could be automated since TFA was not needed in the pre-final-cleavage early steps; the protected amino acids could easily be prepared in high yield and the overall synthesis could be monitored since the fluorine group released from deprotection had UV absorption properties[71,75]

Apart from chemistry, Fmoc SPPS also found wide application in biology since the synthesis could be automated relatively cheaply and hydrogen fluoride would not be needed.[76] Due to these advantages, Fmoc SPPS has been one of the main routes for peptide synthesis since the introduction of SPPS.[71]

1.6 Aims and Objectives

The literature cited thus far displays examples of the self-assembling properties of both linear and cyclic peptides, and methods of obtaining them. These materials could potentially form structures such as hydrogels and organogels. Taking into account the promise of self-assembling cyclic peptides, it is hoped that this study will contribute to the existing body of work. Specifically, the experimental technique/sequence of using Fmoc SPPS to obtain linear peptides, followed by their dissolution and simple heating in the range of solvents used (and

peptide cyclisation characterised), then concluded by revealing their self-assembled formations. Furthermore, it is hoped that more light would be shed on the less-explored self-assembly of cHH, cHF and cHY.

The aim of the project is to address the two problems set out in the overview:

"What is the role of heating solvents in terms of *peptide cyclisation*?" To help answer this, linear peptides will be synthesised, dissolved in different solvents, heated, and the resulting solid products separated from their solvents and experimentally characterised. Comparison of different spectra will confirm whether the end product is different (i.e. whether it is cyclic) to the starting linear peptide.

"Did the *cyclised peptides* subsequently undergo *self-assembly* in the same solvents they were heated in?" To address this, if the solid products obtained beforehand were confirmed to be cyclic, they will be examined by microscopy techniques to observe their overall structure.

With the understanding of intermolecular interactions, possible reasons will be suggested to help understand the formation of these structures based on the solvent environments they were initially in. The effect of solvent polarity on peptide self-assembly will also be suggested, whilst taking into account the unique properties of each solvent. Trends and patterns will be noted between the different peptides and solvents, with comparisons being made to help elucidate the nature of self-assembly for each cyclic dipeptide.

The experimental objectives of this project can be split in two parts:

1) To synthesise four different dipeptide sequences containing different amino acids: *H*-FF-*OH*, *H*-HH-*OH*, *H*-HF-*OH* and *H*-HY-*OH*. Fmoc SPPS with a Wang resin will be employed to achieve this, with all precursor amino acids being Fmoc-protected. These sequences have been specifically chosen because of their varying side-chain aromatic groups.

2) To successfully dissolve the four synthesised dipeptides into solvents of varying polarities and heat them overnight (12 hours). The effect of heating the dipeptides in different solvents will be documented, in relation to peptide cyclisation and self-assembly. Cyclisation will be characterised by MS, NMR and FT-IR. Confirmed cyclic products, which have already been separated from their solvents, will then have their self-assembled structures examined by SEM and optical microscopy.

Chapter Two

Experimental

Chapter 2. Experimental

2.1 Materials

All starting amino acids were Fmoc-protected on the main chain amide (NH_2) groups, and were the *L* isomers.

Chemical	Supplier	Purity
Fmoc-Phe-OH	GL Biochem (Shanghai) Ltd.	≥ 99%
Fmoc-Tyr(tBu)-OH	Fluorochem	98%
Fmoc-His(Trt)-OH	GL Biochem (Shanghai) Ltd.	≥ 99%
Wang resin	GL Biochem (Shanghai) Ltd.	-
HOBt	GL Biochem (Shanghai) Ltd.	≥ 99%
TBTU	GL Biochem (Shanghai) Ltd.	≥ 99%
DMAP	Alfa Aesar	99%
TIS	Alfa Aesar	98%
DIC	Fluorochem	99%
TFA	Fluorochem	99%
HFIP	Fluorochem	99%
DIPEA	Sigma-Aldrich	≥ 99%
Piperidine	Sigma-Aldrich	99%
DMF	Emparta	≥ 99.5%
MeOH	VWR Chemicals	≥ 99.8%
EtOH	VWR Chemicals	≥ 99.8%
n-PrOH	VWR Chemicals	≥ 99.8%
i-PrOH	VWR Chemicals	≥ 99.8%
1,4-Dioxane	Fisher Scientific	≥ 99%
THF	VWR Chemicals	≥ 99.5%
DCM	VWR Chemicals	≥ 99.5%
Et_2O	VWR Chemicals	≥ 99.7%
ACN	Alfa Aesar	99%
n-Hexane	VWR Chemicals	≥ 95%
Toluene	Arcos Organics	99.8%
Water	-	Milli-Q

Table 2. Table showing the chemicals used, along with their purities.

2.2 Instrumentation

Centrifuge

A Heraeus™ Multifuge™ X1 Centrifuge Series was used in obtaining the final linear peptides. The speed was at 5000 rpm.

Heating Oven

A Memmert UF30 oven was used in the cyclisation of the peptides.

Optical Microscope

An Olympus InfinityX BX51 polarising microscope was used to capture images of the samples. To obtain these, four different objective lens (4X, 10X, 20X and 50X) were used, with all the samples at room temperature. Around 10 µl of each solvent containing a self-assembled entity was deposited on a glass slide and examined.

Scanning Electron Microscope

A HITACHI TM 1000 instrument was used, with an accelerating voltage of 15 kV. Samples were deposited on a conductive carbon tape, which was attached to specimen stubs (15 X 10 mm). The stubs were then screwed into the microscope and measurements taken at different magnifications.

Fourier transform infrared spectroscopy

Infrared spectroscopy was used to confirm certain functional groups. A Thermo Scientific™ Nicolet™ iS™5 FT-IR Spectrometer was used with a PIKE Technologies MIRacle™ Single Reflection Horizontal ATR Accessory. Solid samples were placed on a diamond crystal reflection plate and clamped in place by a Micrometer clamp and a swivel tip.

Photoluminescence spectroscopy

One of the self-assembled products was dispersed in more of the solvent it self-assembled in and analysed with a FluoroMax®-4 spectrofluorometer, from HORIBA Scientific.

Mass spectroscopy

Mass spectra were obtained from an Agilent 1100 series HPLC coupled with a Bruker HCT Ultra ion trap MS/MS instrument. The ion source was electrospray, with a capillary voltage of 3.5 kV, gas temp. of 300 °C, and gas flow on 10 L min^{-1}. This was generally used for loop

injections directly into a solvent stream of 5 uL inj. volume. Either positive or negative ion as indicated on the spectrum produced.

Nuclear Magnetic Resonance Spectroscopy

NMR were recorded on a Jeol JNM ECP-400 spectrometer or a Jeol JNM ECZ-S400 spectrometer, with TMS $\delta_H = 0$ as the internal standard or residual protic solvent. Chemical shifts are given in ppm (δ) and coupling constants (J) are given in Hertz (Hz). [$CDCl_3$, δ_H = 7.26; $(CD_3)_2SO$, $\delta_H = 2.50$]. $(CD_3)_2SO$ was used as the solvent for pre-cyclised linear peptides. Cyclised peptides were first dissolved in HFIP (0.5 mL) followed by $CDCl_3$ (1 mL). ^1H NMR were recorded at 400 MHz; ^{13}C recorded at 100.5 MHz with the central peak of $CDCl_3$ (δ_C =77.0 ppm) or $(CD_3)_2SO$ ($\delta_C = 30.8$ ppm) as the internal reference.

Splitting patterns in the spectra are denoted by the following notations:

s - singlet	d - doublet	t - triplet
quart - quartet	quint - quintet	sext - sextet
sept - septet	dd - double doublet	qd - quartet of doublets
m - multiplet	br - broad	

2.3 Linear peptide synthesis protocol

The procedure below follows the standard protocol, and a brief description is given for each coupling agent. All reactions were performed at room temperature.

Wang resin was added to a reaction vessel. The solvent used for all reagents is DMF. Relative to a weighed amount of the resin, the following chemicals were added in different equivalencies.

- Fmoc-protected amino acid: **2 mol. eq. reagent to 1.2 mmolg^{-1} Wang resin**
- DIC: **2 mol. eq. reagent to 1.2 mmolg^{-1} Wang resin**
- HOBt: **2 mol. eq. reagent to 1.2 mmolg^{-1} Wang resin**
- DMAP: **0.2 mol. eq. reagent to 1.2 mmolg^{-1} Wang resin**
- TBTU: **2 mol. eq. reagent to 1.2 mmolg^{-1} Wang resin**
- DIPEA: **2 mol. eq. reagent to 1.2 mmolg^{-1} Wang resin**

The scales used below are typical masses/moles.

Resin swelling:

15 mL DCM was added to the resin (5 g, 6.0 mmol, 1.2 mmolg^{-1}) and left for 15 min.

1st Amino Acid Coupling:

Fmoc-AA-*OH* (4.5 g, 11.6 mmol) (where -AA- represents any two amino acids), DIC (1.8 mL, 11.6 mmol), HOBt (1.6 g) and DMAP (0.1 g, 1.2 mmol) were dissolved in DMF. This was added to the resin and left overnight.

1st Fmoc Deprotection:

The vessel was washed 5 times with DMF. 15 mL 20% piperidine in DMF was added to resin and left for 20 min. It was then washed 5 times with DMF.

2nd Amino Acid Coupling:

Fmoc-AA-*OH* (4.5 g, 11.6 mmol), TBTU (3.7 g, 11.6 mmol), HOBt (1.6 g, 11.6 mmol) and DIPEA (2 mL, 11.6 mmol) were dissolved in DMF. This was added to the resin and left for 45 min.

2nd Fmoc Deprotection:

The vessel was washed 5 times with DMF. 15 mL 20% piperidine in DMF was added to the resin and left for 20 min. This was washed 5 times with DMF, then 5 times with DCM. The resin was dried under a vacuum for 2 hr.

Cleavage:

A 30 mL cleavage solution containing TFA (27.6 mL), TIS (1.2 mL) and H_2O (1.2 mL) in the ratio 92:4:4 was prepared. The solution was added to the resin and left for 2 h.

Product Isolation:

The solution was filtered and precipitated with ice-cold Et_2O (100 mL). A precipitate was observed. The solution with the precipitate were centrifuged. Et_2O was decanted off, fresh Et_2O was added and centrifuged again. This was repeated 3 times.

Fig. 10 is a schematic depiction of the process.

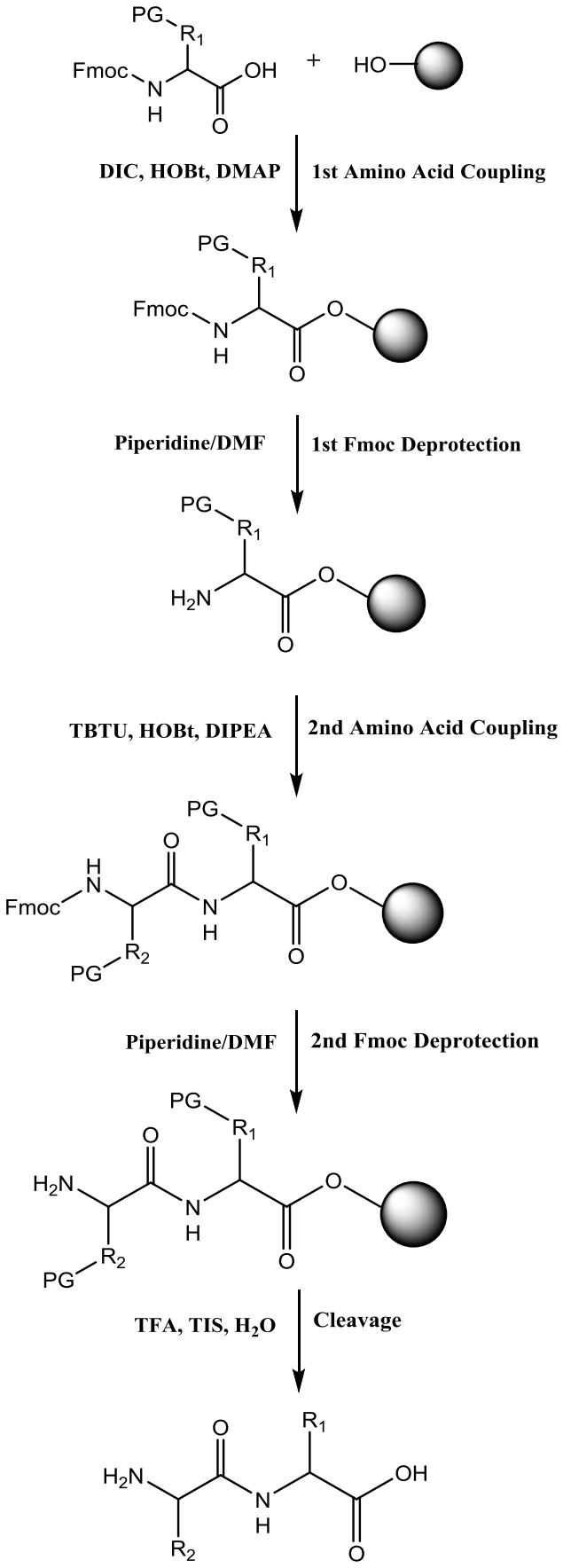

Figure 10. Schematic diagram[77] of the SPPS process used in this project.

2.4 Linear peptides

The following procedures all follow the peptide synthesis protocol in 2.3.

2.4.1. *H*-FF-*OH*

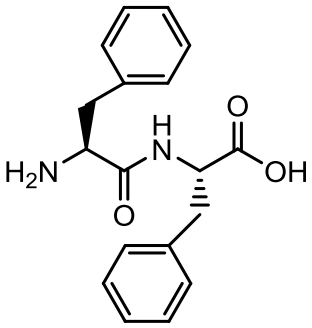

Figure 11. Molecular structure of H-FF-OH.

Procedure: Fmoc-Phe-*OH* (4.5 g, 11.6 mmol) was coupled to a Wang resin (5 g, 6.0 mmol, 1.2 $mmolg^{-1}$) via the reagents DIC (1.8 mL, 11.6 mmol), HOBt (1.6 g, 11.6 mmol) and DMAP (0.1 g, 1.2 mmol). The Fmoc group was deprotected by 15 mL 20% piperidine/DMF. The second Fmoc-Phe-*OH* (4.5 g, 11.6 mmol) was coupled to the first amino acid via the reagents TBTU (3.7 g, 11.6 mmol), HOBt (1.6 g, 11.6 mmol) and DIPEA (2 mL, 11.6 mmol). The Fmoc group was deprotected by 15 mL 20% piperidine/DMF. The peptide was cleaved by a solution of 27.6 mL TFA, 1.2 mL TIS and 1.2 mL H_2O, and precipitated by 100 mL Et_2O.

The white solid was obtained in a 51% yield (0.9 g).

MS m/z (ESI): Calculated for $C_{18}H_{20}N_2O_3$ ($[M]^+$): 312.37. Obtained: 313.14 $[M + H^+]^+$, 625.29 $[2M + H^+]^+$, 937.53 $[3M + H^+]^+$.

Literature[78] MS m/z (ESI): 313 $[M + H^+]^+$, 335 $[M + Na]^+$, 625 $[2M + H^+]^+$, 647 $[2M + Na]^+$.

^{1}H NMR ($(CD_3)_2SO$, 400 MHz) δ_H: 8.86 (2H, d, J = 7.79 Hz, NH_2), 8.16 (1H, br, NH), 7.20 (10H, m, ArH), 4.48 (1H, m, COOH-CH), 4.03 (1H, quart, NH_2-CH), 3.33 - 2 .91 (4H, m, CH_2).

Literature[78] ^{1}H NMR ($(CD_3)_2SO$, 400 MHz) δ_H: 7.35 - 7.24 (10H, m), 4.52 (1H, dd, J_1 = 8.1 Hz, J_2 = 4.8 Hz), 3.99 (1H, dd, J_1 = 9.0 Hz, J_2 = 4.8 Hz), 3.28 - 3.22 (2H, m), 3.02 (1H, dd, J_1 = 13.9 Hz, J_2 = 8.1 Hz), 2.92 (1H, dd, J_1 = 14.4 Hz, J_2 = 9.0 Hz).

^{13}C NMR ((CD$_3$)$_2$SO, 100.5 MHz) δ_C: 172.8 (COOH), 168.7 (CO), 137.7 (ArC), 129.9 (ArCH), 129.0 (ArCH), 127.2 (ArCH), 54.3 (COOH-CH), 53.7 (NH_2-CH), 37.4 (CH_2), 37.3 (CH_2).

IR ν_{max}/cm^{-1}: 2872, 1722, 1688, 1569, 1547, 1496, 1456, 1427, 1282, 1137, 1094, 1033, 992, 919, 840, 797, 747, 741, 723, 700, 629.

The mass and ^{1}H NMR results agree well with the reported data.[78] The ^{13}C NMR values are also in agreement with the reported literature.[79]

2.4.2. *H*-HH-*OH*

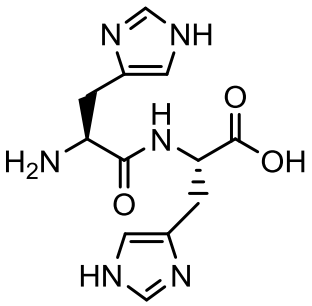

Figure 12. Molecular structure of H-HH-OH.

Procedure: Fmoc-His(Trt)-*OH* (14.4 g, 23.2 mmol) was coupled to a Wang resin (10 g, 11.6 mmol, 1.2 $mmolg^{-1}$) via the reagents DIC (3.6 mL, 23.2 mmol), HOBt (3.1 g, 23.2 mmol) and DMAP (0.3 g, 2.3 mmol). The Fmoc group was deprotected by 15 mL 20% piperidine/DMF. The second Fmoc-His(Trt)-*OH* (14.4 g, 23.2 mmol) was coupled to the first amino acid via the reagents TBTU (7.4 g, 23.2 mmol), HOBt (3.1 g, 23.2 mmol) and DIPEA (4 mL, 23.2 mmol). The Fmoc group was deprotected by 15 mL 20% piperidine/DMF. The peptide was cleaved by a solution of 36.8 mL TFA, 1.6 mL TIS and 1.6 mL H_2O, and precipitated by 100 mL Et_2O.

The white solid was obtained in a 127% yield (4.3 g).

MS m/z (ESI): Calculated for $C_{12}H_{16}N_6O_3$ ($[M]^+$): 292.30. Obtained: 274.94 $[M - H_2O]^+$, 292.97 $[M + H^+]^+$.

^{1}H NMR ($(CD_3)_2SO$, 400 MHz) δ_H: 8.98 (2H, d, J = 7.34 Hz, NH_2), 8.85 (2H, m, ArH), 8.29 (1H, s, NH), 7.91 (2H, s, ArH), 4.57, (1H, br, COOH-CH), 4.13 (1H, t, J = 5.96 Hz, NH_2-CH), 3.01 (4H, m, CH_2).

^{13}C NMR ($(CD_3)_2SO$, 100.5 MHz) δ_C: 172.0 (COOH), 168.1 (CO), 135.1 (ArCH), 129.8 (ArC), 128.8, 127.9 (ArC), 117.5 (ArCH), 52.3 (COOH-CH), 51.8 (NH_2-CH), 27.1 (CH_2), 26.9 (CH_2).

IR ν_{max}/cm^{-1}: 2862, 1666, 1434, 1189, 1130, 976, 835, 797, 667, 630.

2.4.3. *H*-HF-*OH*

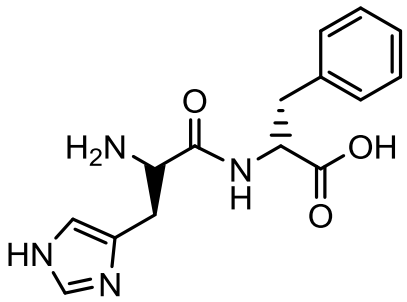

Figure 13. Molecular structure of H-HF-OH.

Procedure: Fmoc-Phe-*OH* (8.9 g, 23.2 mmol) was coupled to a Wang resin (10 g, 11.6 mmol, 1.2 $mmolg^{-1}$) via the reagents DIC (3.6 mL, 23.2 mmol), HOBt (3.1 g, 23.2 mmol) and DMAP (0.3 g, 2.3 mmol). The Fmoc group was deprotected by 15 mL 20% piperidine/DMF. Fmoc-His(Trt)-*OH* (14.4 g, 23.2 mmol) was coupled to the first amino acid via the reagents TBTU (7.4 g, 23.2 mmol), HOBt (3.1 g, 23.2 mmol) and DIPEA (4 mL, 23.2 mmol). The Fmoc group was deprotected by 15 mL 20% piperidine/DMF. The peptide was cleaved by a solution of 36.8 mL TFA, 1.6 mL TIS and 1.6 mL H_2O, and precipitated by 100 mL Et_2O.

The white solid was obtained in a 51% yield (1.8 g).

MS m/z (ESI): Calculated for $C_{15}H_{18}N_4O_3$ ($[M]^+$): 302.33. Obtained: 284.99 $[M - H_2O]^+$, 303.00 $[M + H^+]^+$, 605.13 $[2M + H^+]^+$.

^1H NMR ($(CD_3)_2SO$, 400 MHz) δ_H: 8.83 (2H, d, J = 7.79 Hz, NH_2), 8.71 (1H, s, ArH), 8.31 (1H, s, NH), 7.95 (1H, s, ArH), 7.18 (5H, m, ArH), 4.46 (1H, s, COOH-CH), 4.08 (1H, s, NH_2-CH), 3.09 - 2.85 (4H, m, CH_2).

^{13}C NMR ($(CD_3)_2SO$, 100.5 MHz) δ_C: 172.9 (COOH), 168.2 (CO), 137.8 (ArC), 135.1 (ArCH), 129.7 (ArC), 128.8 (ArCH), 128.3 (ArCH), 127.1 (ArCH), 118.1 (ArCH), 54.6 (COOH-CH), 51.8 (NH_2-CH), 36.3 (CH_2), 31.3 (CH_2).

IR ν_{max}/cm^{-1}: 2868, 1660, 1538, 1433, 1184, 1131, 971, 916, 835, 797, 700, 667, 627.

2.4.4. *H*-HY-*OH*

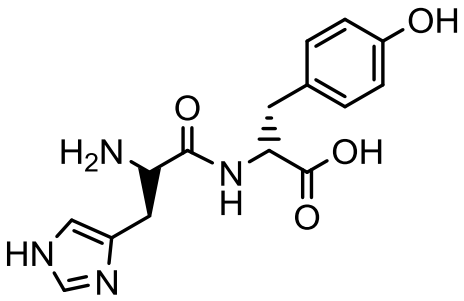

Figure 14. Molecular structure of H-HY-OH.

Procedure: Fmoc-Tyr(tBu)-*OH* (10.7 g, 23.2 mmol) was coupled to a Wang resin (10 g, 11.6 mmol, 1.2 $mmolg^{-1}$) via the reagents DIC (3.6 mL, 23.2 mmol), HOBt (3.1 g, 23.2 mmol) and DMAP (0.3 g, 2.3 mmol). The Fmoc group was deprotected by 15 mL 20% piperidine/DMF. Fmoc-His(Trt)-*OH* (14.4 g, 23.2 mmol) was coupled to the first amino acid via the reagents TBTU (7.4 g, 23.2 mmol), HOBt (3.1 g, 23.2 mmol) and DIPEA (4 mL, 23.2 mmol). The Fmoc group was deprotected by 15 mL 20% piperidine/DMF. The peptide was cleaved by a solution of 36.8 mL TFA, 1.6 mL TIS and 1.6 mL H_2O, and precipitated by 100 mL Et_2O.

The white solid was obtained in a 63% yield (2.3 g).

MS m/z (ESI): Calculated for $C_{15}H_{18}N_4O_4$ ($[M]^+$): 318.33. Obtained: 301.10 $[M - H_2O]^+$, 319.04 $[M + H^+]^+$.

^1H NMR ($(CD_3)_2SO$, 400 MHz) δ_H: 8.83 (2H, m, NH_2), 8.75 (1H, d, J = 7.79 Hz, ArH), 8.23 (1H, s, NH), 7.91 (1H, s, ArH), 6.97 (2H, m, o-ArH), 6.72 - 6.62 (2H, m, m-ArH), 4.33 (1H, s, COOH-CH), 4.10 (1H, s, NH_2-CH), 3.17 - 2.69 (4H, m, CH_2).

^{13}C NMR ($(CD_3)_2SO$, 100.5 MHz) δ_C: 173.0 (COOH), 168.1 (CO), 156.6 (COH), 135.1 (ArCH), 130.1 (ArC), 128.5 (o-ArCH), 127.6 (ArC), 118.0 (ArCH), 115.6 (m-ArCH), 54.9 (COOH-CH), 51.8 (NH_2-CH), 36.3 (CH_2), 31.3 (CH_2).

IR ν_{max}/cm^{-1}: 2877, 2278, 1660, 1515, 1435, 1388, 835, 797, 721, 665, 626.

2.5 Cyclic peptides

All linear peptides were added to their solvents in a 10 mg/mL concentration. Below are the characterisations for any self-assembled solids that were formed. More detail will be discussed in chapter 3.

2.5.1. cFF/H_2O

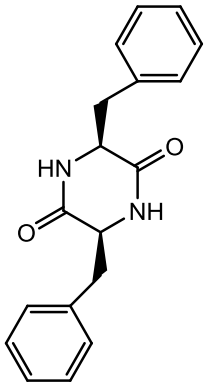

Figure 15. Molecular structure of cFF.

H-FF-*OH* (0.2 g) was dissolved in H_20 (20 mL), and heated to 90 °C for 12 h.

The end product was filtered from its solvent and air-dried (left after vacuum Büchner filtration) to give a 33% yield (0.1 g).

MS m/z (ESI): Calculated for $C_{18}H_{18}N_2O_2$ ($[M]^+$): 294.35. Obtained: 295.10 $[M + H^+]^+$, 313.10 $[M + H_2O + H^+]^+$.

Literature[80] MALDI-TOF MS m/z: 295.064 $[M + H^+]^+$.

^{1}H NMR ($CDCl_3$, 400 MHz) δ_H: 7.36 (10H, m, ArH), 4.35 (2H, m, NH-CH), 2.91 (4H, dd, J = 3.67, 13.75 Hz, CH_2).

^{13}C NMR ($CDCl_3$, 100.5 MHz) δ_C: 168.3 (CO), 133.9 (ArC), 129.5 (ArCH), 128.1 (ArCH), 125.5 (ArCH), 56.3 (NH-CH), 39.6 (CH_2).

IR ν_{max}/cm^{-1}: 3052, 2360, 1658, 1496, 1454, 1349, 1337, 1267, 1211, 1194, 1091, 1032, 1014, 920, 899, 853, 802, 755, 658.

The MS results agree with that of the literature.[80,81] The ^{13}C NMR values also concur with the reported data for the (S,S) isomer[79] and (R,S) isomer,[82] but more closely match the former in terms of the (CH_2) peak.

2.5.2. cFF/EtOH

H-FF-*OH* (0.1 g) was dissolved in EtOH (10 mL), and heated to 68 °C for 12 h.

The end product was filtered from its solvent and air-dried (left after vacuum Büchner filtration) to give a 34% yield (0.03 g).

MS m/z (ESI): Calculated for $C_{18}H_{18}N_2O_2$ ($[M]^+$): 294.35. Obtained: 295.10 $[M + H^+]^+$, 317.10 $[M + Na]^+$, 589.20 $[2M + H^+]^+$.

^{1}H NMR ($CDCl_3$, 400 MHz) δ_H: 7.38 (10H, m, ArH), 4.37 (2H, m, NH-CH), 2.93 (4H, dd, J = 13.98, 3.67 Hz, CH_2).

^{13}C NMR ($CDCl_3$, 100.5 MHz) δ_C: 168.4 (CO), 133.9 (ArC), 129.4 (ArCH), 128.0 (ArCH), 125.4 (ArCH), 56.3 (NH-CH), 39.5 (CH_2).

IR ν_{max}/cm^{-1}: 3054, 2348, 1658, 1497, 1459, 1337, 1267, 1211, 1091, 1015, 921, 899, 803, 755, 699, 659.

2.5.3. cFF/n-PrOH

H-FF-*OH* (0.1 g) was dissolved in n-PrOH (10 mL), and heated to 87 °C for 12 h.

The end product was filtered from its solvent and air-dried (left after vacuum Büchner filtration) to give a 54% yield (0.1 g).

MS m/z (ESI): Calculated for $C_{18}H_{18}N_2O_2$ ($[M]^+$): 294.35. Obtained: 295.10 $[M + H^+]^+$, 317.10 $[M + Na]^+$, 589.20 $[2M + H^+]^+$.

^{1}H NMR ($CDCl_3$, 400 MHz) δ_H: 7.39 (10H, m, ArH), 4.39 (2H, m, NH-CH), 2.93 (4H, dd, J = 13.75, 3.67 Hz, CH_2).

^{13}C NMR ($CDCl_3$, 100.5 MHz) δ_C: 168.4 (CO), 133.9 (ArC), 129.4 (ArCH), 128.0 (ArCH), 125.4 (ArCH), 56.4 (NH-CH), 39.5 (CH_2).

IR ν_{max}/cm^{-1}: 3053, 1658, 1497, 1459, 1349, 1338, 1267, 1211, 1194, 1091, 1033, 1015, 921, 899, 853, 802, 755, 659.

2.5.4. cFF/i-PrOH

H-FF-*OH* (0.1 g) was dissolved in i-PrOH (10 mL), and heated to 72 °C for 12 h.

The end product was filtered from its solvent and air-dried (left after vacuum Büchner filtration) to give a 52% yield (0.1 g).

MS m/z (ESI): Calculated for $C_{18}H_{18}N_2O_2$ ($[M]^+$): 294.35. Obtained: 295.10 $[M + H^+]^+$, 313.10 $[M + H_2O + H^+]^+$, 335.10 $[M + H_2O + Na]^+$.

^{1}H NMR ($CDCl_3$, 400 MHz) δ_H: 7.37 (10H, m, ArH), 4.36 (2H, m, NH-CH), 2.92 (4H, dd, J = 14.21, 3.67 Hz, CH_2).

^{13}C NMR ($CDCl_3$, 100.5 MHz) δ_C: 168.3 (CO), 133.9 (ArC), 129.5 (ArCH), 128.0 (ArCH), 125.4 (ArCH), 56.4 (NH-CH), 39.6 (CH_2).

IR ν_{max}/cm^{-1}: 3196, 3053, 1659, 1497, 1460, 1349, 1338, 1268, 1211, 1194, 1091, 1033, 1015, 921, 899, 853, 803, 699, 659.

2.5.5. cFF/1,4-dioxane

H-FF-*OH* (0.1 g) was dissolved in 1,4-dioxane (10 mL), and heated to 90 °C for 12 h.

The end product was filtered from its solvent and air-dried (left after vacuum Büchner filtration) to give a 47% yield (0.04 g).

MS m/z (ESI): Calculated for $C_{18}H_{18}N_2O_2$ ($[M]^+$): 294.35. Obtained: 295.10 $[M + H^+]^+$, 317.10 $[M + Na]^+$, 589.20 $[2M + H^+]^+$.

^{1}H NMR ($CDCl_3$, 400 MHz) δ_H: 7.38 (10H, m, ArH), 4.36 (2H, m, NH-CH), 2.93 (4H, dd, J = 13.75, 3.67 Hz, CH_2).

^{13}C NMR ($CDCl_3$, 100.5 MHz) δ_C: 168.3 (CO), 133.9 (ArC), 129.5 (ArCH), 128.0 (ArCH), 125.4 (ArCH), 56.4 (NH-CH), 39.6 (CH_2).

IR ν_{max}/cm^{-1}: 3052, 2358, 2164, 1659, 1497, 1460, 1338, 1267, 1211, 1091, 1015, 921, 899, 804, 699, 659.

2.5.6. cFF/THF

H-FF-*OH* (0.1 g) was dissolved in THF (10 mL), and heated to 56 °C for 12 h.

The end product was filtered from its solvent and air-dried (left after vacuum Büchner filtration) to give a 49% yield (0.04 g).

MS m/z (ESI): Calculated for $C_{18}H_{18}N_2O_2$ ($[M]^+$): 294.35. Obtained: 295.10 $[M + H^+]^+$.

^{1}H NMR ($CDCl_3$, 400 MHz) δ_H: 7.37 (10H, m, ArH), 4.35 (2H, m, NH-<u>CH</u>), 2.91 (4H, dd, J = 13.75, 3.67 Hz, CH_2).

^{13}C NMR ($CDCl_3$, 100.5 MHz) δ_C: 168.3 (CO), 133.9 (ArC), 129.5 (ArCH), 128.1 (ArCH), 125.5 (ArCH), 56.3 (NH-<u>CH</u>), 39.6 (CH_2).

IR ν_{max}/cm^{-1}: 3198, 1674, 1660, 1497, 1460, 1338, 1268, 1212, 1091, 1015, 921, 899, 805, 700, 660.

2.5.7. cHH/n-PrOH

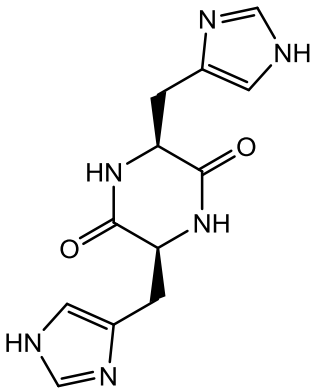

Figure 16. Molecular structure of cHH.

H-HH-*OH* (0.2 g) was dissolved in n-PrOH (20 mL), and heated to 87 °C for 12 h.

The end product was filtered from its solvent and air-dried (left after vacuum Büchner filtration) to give a 39% yield (0.1 g).

MS m/z (ESI): Calculated for $C_{12}H_{14}N_6O_2$ ($[M]^+$): 274.28. Obtained: 274.97 $[M + H^+]^+$, 549.13 $[2M + H^+]^+$.

^{1}H NMR ($CDCl_3$, 400 MHz) δ_H: 8.28 (2H, s, ArH), 8.13 (2H, s, NH), 7.33 (2H, s, ArH), 4.13 (2H, s, NH-CH), 3.30 (2H, t, J = 6.42 Hz, CH_2), 2.79 (2H, m, CH_2).

^{13}C NMR ($CDCl_3$, 100.5 MHz) δ_C: 167.5 (CO), 134.9 (ArCH), 131.2 (ArC), 117.8 (ArCH), 54.4 (NH-CH), 29.5 (CH_2).

IR ν_{max}/cm^{-1}: 3109, 1979, 1662, 1621, 1455, 1332, 1269, 1232, 1202, 1108, 1090, 990, 936, 831, 774, 743, 721, 649, 638, 627.

The ^{1}H NMR values agree with the (S,S) isomer reported in the literature.[83]

2.5.8. cHF/i-PrOH

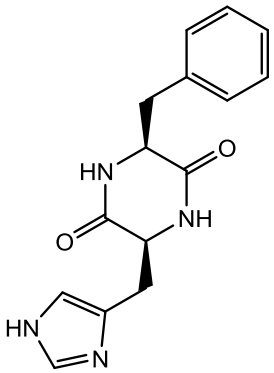

Figure 17. Molecular structure of cHF.

H-HF-*OH* (0.2 g) was dissolved in i-PrOH (20 mL), and heated to 72 °C for 12 h.

The end product was filtered from its solvent and air-dried (left after vacuum Büchner filtration) to give a 39% yield (0.1 g).

MS m/z (ESI): Calculated for $C_{15}H_{16}N_4O_2$ ($[M]^+$): 284.32. Obtained: 285.00 [M + H^+], 307.00 $[M + Na]^+$.

^{1}H NMR ($CDCl_3$, 400 MHz) δ_H: 8.19 (2H, s, NH), 7.25 (1H, s, ArH), 7.18 (5H, d, J = 7.79 Hz, ArH), 4.38 (2H, m, NH-CH), 3.16 (4H, qd, J = 4.58 Hz, 14.21 Hz, CH_2).

^{13}C NMR ($CDCl_3$, 100.5 MHz) δ_C: 168.0 (CO), 133.3 (ArC), 132.9 (ArCH) 130.2 (ArC), 128.5 (ArCH), 128.3 (ArCH), 125.5 (ArCH), 117.2 (ArCH), 56.2 (NH-CH), 39.0 (CH_2), 28.6 (CH_2).

IR ν_{max}/cm^{-1}: 3428, 3032, 2875, 1660, 1463, 1336, 1199, 1137, 1095, 1001, 946, 908, 835, 796, 767, 721, 702, 679, 629.

The MS, ^{1}H NMR, ^{13}C NMR and IR values agree with the (S,S) isomer in the reported literature.[20]

2.5.9. cHF/THF

H-HF-*OH* (0.2 g) was dissolved in THF (20 mL), and heated to 56 °C for 12 h.

The end product was filtered from its solvent and air-dried (left after vacuum Büchner filtration) to give a 34% yield (0.1 g).

MS m/z (ESI): Calculated for $C_{15}H_{16}N_4O_2$ ($[M]^+$): 284.32. Obtained: 284.96 $[M + H^+]^+$, 569.13 $[2M + H^+]^+$.

^{1}H NMR ($CDCl_3$, 400 MHz) δ_H: 7.25 (1H, s, ArH), 7.04 (5H, d, J = 6.88 Hz, ArH), 4.35 (2H, m, NH-CH) 2.60 (4H, s, CH_2).

^{13}C NMR ($CDCl_3$, 100.5 MHz) δ_C: 168.2 (CO), 133.9 (ArC), 129.7 (ArCH), 129.3 (ArC), 128.1 (ArCH), 125.5 (ArCH), 122.7 (ArCH), 117.1 (ArCH), 56.3 (NH-CH), 39.6 (CH_2).

IR ν_{max}/cm^{-1}: 3432, 3032, 2876, 2629, 1660, 1633, 1464, 1423, 1341, 1320, 1238, 1201, 1176, 1158, 1140, 1094, 1001, 945, 909, 834, 795, 775, 721, 703, 679, 630.

2.5.10. cHY/i-PrOH

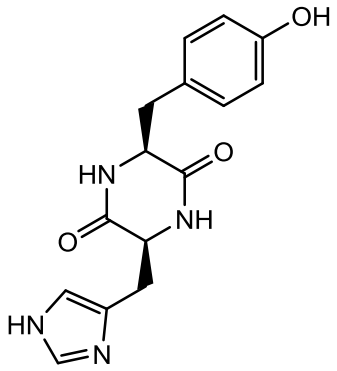

Figure 18. Molecular structure of cHY.

H-HY-*OH* (0.2 g) was dissolved in i-PrOH (20 mL), and heated to 72 °C for 12 h.

The end product was filtered from its solvent and air-dried (left after vacuum Büchner filtration) to give a 36% yield (0.1 g).

MS m/z (ESI): Calculated for $C_{15}H_{16}N_4O_3$ ($[M]^+$): 300.32. Obtained: 301.09 $[M + H^+]^+$.

^{1}H NMR ($(CD_3)_2SO$, 400 MHz) δ_H: 8.85 (1H, s, ArH), 8.23 (2H, s, NH), 7.97 (1H, s, ArH), 7.03 (2H, t, J = 8.25 Hz, o-ArH), 6.63 (2H, d, J = 7.34 Hz, m-ArH), 2.92 (2H, d, J = 11.0 Hz, CH_2), 2.70 (2H, dd, J = 13.53, 4.58 Hz, CH_2).

^{13}C NMR ($(CD_3)_2SO$, 100.5 MHz) δ_C: 166.9 (CO), 156.9 (ArCOH), 134.9 (ArCH), 131.9 (ArC), 129.1 (o-ArCH), 126.5 (ArC), 117.7 (ArCH), 115.6 (m-ArCH), 56.1 (NH-CH), 38.2 (CH_2), 29.9 (CH_2).

IR ν_{max}/cm^{-1}: 3055, 1661, 1513, 1456, 1332, 1240, 1212, 1198, 1177, 1119, 1023, 953, 880, 836, 770, 751, 721, 677, 630.

The ^{1}H NMR values agree with the (S,S) isomer reported in the literature.[83]

2.5.11. cHY/THF

H-HY-*OH* (0.2 g) was dissolved in THF (20 mL), and heated to 56 °C for 12 h.

The end product was filtered from its solvent and air-dried (left after vacuum Büchner filtration) to give a 42% yield (0.1 g).

MS m/z (ESI): Calculated for $C_{15}H_{16}N_4O_3$ ($[M]^+$): 300.32. Obtained: 301.10 $[M + H^+]^+$.

^{1}H NMR ($(CD_3)_2SO$, 400 MHz) δ_H: 8.83 (1H, s, ArH), 8.22 (2H, s, NH), 7.96 (1H, s, ArH), 6.89 (2H, t, o-ArH), 6.64 (2H, d, J = 6.42 Hz, m-ArH), 2.93 (2H, d, J = 13.75 Hz, CH_2), 2.70 (2H, d, J = 13.75 Hz, CH_2).

^{13}C NMR ($(CD_3)_2SO$, 100.5 MHz) δ_C: 166.9 (CO), 156.9 (ArCOH), 134.9 (ArCH), 131.9 (ArC), 129.1 (o-ArCH), 126.5 (ArC), 117.7 (ArCH), 115.6 (m-ArCH), 56.2 (NH-CH), 38.2 (CH_2), 29.9 (CH_2).

IR ν_{max}/cm^{-1}: 3052, 2880, 2076, 2014, 1979, 1662, 1514, 1457, 1337, 1236, 1177, 1135, 1048, 952, 910, 834, 795, 771, 750, 721, 679, 629.

Chapter Three

Results and Discussion

Chapter 3. Results and Discussion

3.1 Synthesis

Figure 19. Big SPPS reaction vessel on left, small SPPS reaction vessel on right; both loaded with Wang resin.

Customised apparatus were used as the reaction vessels, as seen in Fig. 19: The resin and solvents are introduced in the vessel through the top. For efficient reactions, the closed vessel is then manually shaken by hand for a certain period of time. Next, the solution is vacuum-filtered into the round bottom flask below. This general system is repeated after the introduction of each new solvent and cleavage solution. No part of this process was automated.

The following details the role of each reagent used in **2.3**:

1st Coupling: DIC and HOBt are both involved in the carboxy activation of the first amino acid. In addition, HOBt minimizes any partial racemization of the amino acid caused by the activation. DMAP is a catalyst which is needed in general for coupling amino acids to a hydroxy-functionalized resin. 0.2 eq is used since larger amounts can cause racemization.[75] The activated amino acid is then coupled to the resin.

Deprotection: Piperidine is a base used to remove the Fmoc group.

2nd Coupling: TBTU and HOBt are involved in the carboxy activation of the second amino acid, however TBTU requires the presence of a base to react.[75] This requirement is met by DIPEA (Hünig's base). The second activated amino acid can then couple with the first one already linked to the resin.

Cleavage: TFA cleaves the bond between the resin and the amino acid chain, thus releasing the new peptide. The acid also deprotects side chain protecting groups that are acid-labile, e.g. –Trt. TIS and water are nucleophilic scavengers, used to quench any reactive cationic species produced from the cleavage of protecting groups and the resin linker.

The synthesis of *H*-FF-*OH* and *H*-HF-*OH* gave the same yield (51 %), whereas *H*-HY-*OH* had a higher yield of 63%. In general, incomplete deprotection by piperidine and/or incomplete coupling could result in loss of material to give the 51%/63% yields. Inadequate cleavage may also contribute to this. Although only dipeptides were synthesised, it is usual for each successive amino acid coupling in SPPS to result in a decreased final yield. *H*-HH-*OH* gave a 127% yield, and a possible reason for this could be due to the histidine groups reacting with TFA to give a salt in addition to the final peptide. This yield could be reduced by purification. For this project, the yields were sufficient to produce enough peptide for experimentation.

The linear peptides were first added into empty sample vials followed by each solvent. For the solvents that the peptides were confirmed to dissolve in completely in the following sections (3.2 – 3.5), it was seen that the *H*-FF-*OH* and *H*-HF-*OH* dissolved instantly in those solvents. The dissolution of *H*-HH-*OH* and *H*-HY-*OH* was not instantaneous and was aided by the use of a sonicator. All the vials had PTFE-lined caps in order to withstand the higher heating temperatures, e.g. 90 °C. After the samples were heated in the oven, they were allowed to return to room temperature before they were analysed.

3.2 cFF

For all the dipeptides in this work, the general process is that they first cyclise via heating, then subsequently self-assemble in their solvents.

Given the recent research around diphenylalanine, noted in **1.2**, its tendency to form nanotubes under various conditions is known. Apart from water, however, little is known concerning its self-assembly in other solvents; and more specifically, via the cyclisation method in this project.

To start off this study, the self-assembly of cFF in water (cyclised from *H*-FF-*OH* via heating) was investigated to see what structures form compared to the existing literature. Likewise, the rest of the solvents were tested in a similar fashion. This is an interesting aspect because it could potentially show if the particular self-assembly of cFF displays similar formations in different solvents.

Referring back to **1.4**, amide formation from amine/carboxylic acid precursors via simple heating is unusual and conventionally proceeds by organic chemical synthesis. It is speculated that the driving force behind the unconventional cyclisation in the following experiments is the formation of the more energetically favoured cyclic derivative,[58] followed by the loss of water.[54-57]

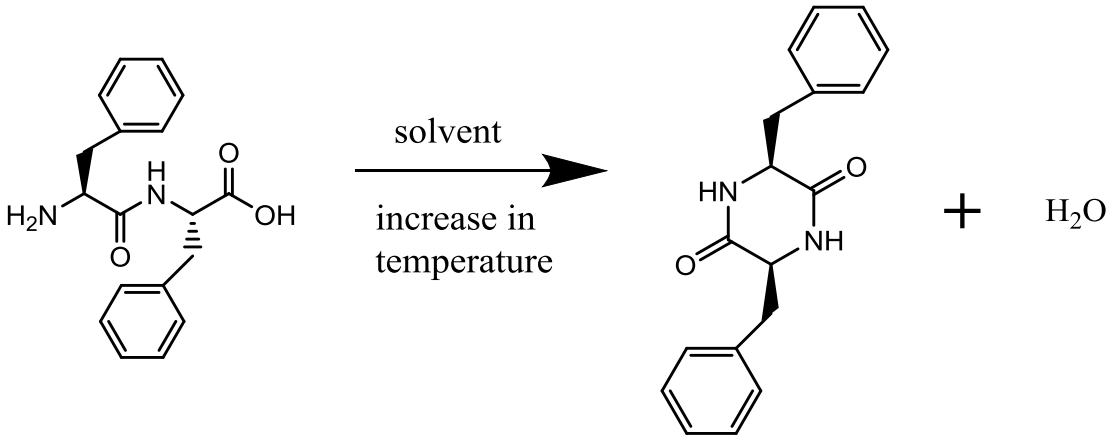

Figure 20. Proposed schematic diagram of H-FF-OH cyclisation. Terminal carboxylic acid and amine groups join together during heating to form a cyclic amide bond.

Jaworska et al. conducted an investigation where a muffle furnace was used to heat *H*-FF-*OH* nanotubes at 423 K (149.85 °C), for 30 min, to give cFF nanotubes.[79] Solid state cross-polarization magic angle spinning ^{13}C CP/MAS NMR spectra were obtained for both the initial *H*-FF-*OH* and cFF nanotubes, and the geometry of their cFF was revealed to be the cis isomer.[79] In this project, no experimental techniques were utilised to ascertain any optical rotations. However, referring back to **2.5.1.**, when comparing the lit. data for (S,S)[79] to that of (R,S)[82], the obtained ^{13}C NMR values more closely match the (S,S) in terms of the proton environment between the phenyl and cyclic amide ring (CH_2). From this information, it is assumed that the (S,S) configuration has not changed.

The overall scheme of the whole self-assembly process is:

H-FF-*OH* dissolves in solvent → Solvent containing *H*-FF-*OH* is heated → *H*-FF-*OH* cyclises to give cFF in solvent (due to heating) → cFF self-assembles in same solvent.

This routine applies to the other dipeptide sequences.

The following table and picture shows the results of heating *H*-FF-*OH* samples in different solvents:

Solvent	**Peptide dissolution and solution appearance**	**Appearance after 12 h heating**
H_2O	Dissolved, colourless	White aggregate
EtOH	Dissolved, colourless	White aggregate
n-PrOH	Dissolved, colourless	White aggregate
i-PrOH	Dissolved, colourless	White aggregate
THF	Dissolved, colourless	White aggregate
1,4-Dioxane	Dissolved, colourless	White aggregate
Toluene	Insoluble	-
n-Hexane	Insoluble	-

Table 3. Results of H-FF-OH dissolution and appearance after heating.

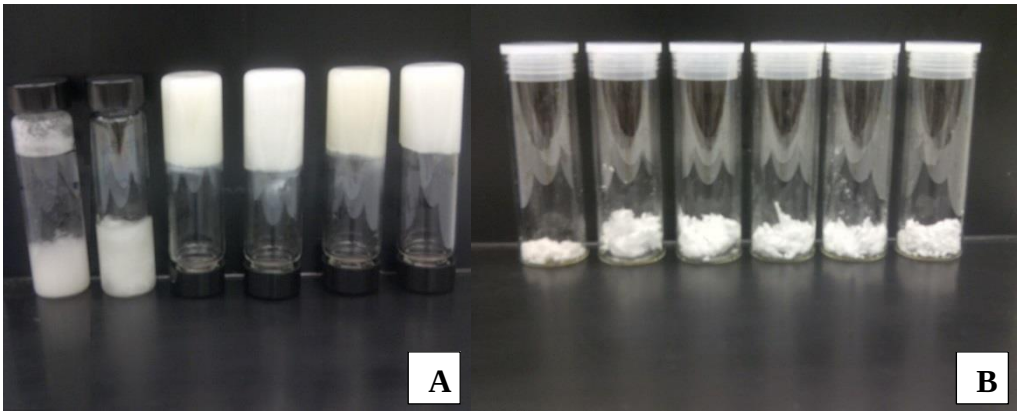

Figure 21. Sample vials of dissolved H-FF-OH after heating (hence aggregates are cFF). (A) was taken immediately after heating whereas (B) was taken when each product was filtered from their solvent. For both images, samples from left to right contained the solvents H_2O, EtOH, n-PrOH, i-PrOH, THF and 1,4-dioxane.

After isolating the compounds seen in Fig. 21a, they had the appearance of white solid aggregates; Fig. 21b.

The solid self-assembled aggregates obtained after the heating were confirmed to be cyclic by the characterisation methods in the experimental section. This characterisation will be detailed below, and also be discussed for the other dipeptides.

On comparing the characterisation of the starting *H*-FF-*OH* peptide, in **2.4.1.**, with that of the white aggregates, **2.5.1. - 2.5.6.**, the following is observed. The IR peaks arising from *H*-FF-*OH* and the aggregates are not that distinct from each other, because of the similar amino/carbonyl groups. The differences in the mass and NMR spectra peaks are more prominent. The protonated molecular ion peak observed for the preheated dipeptide, 313.14 $[M + H^+]^+$, is different than that of each of the aggregates, 295.10 $[M + H^+]^+$ (the exact m/z seen for all six). The calculated mass for cFF is 294.35 ($[M]^+$). The total number of proton and carbon NMR peaks observed for the aggregates are lower than the preheated dipeptide, which is expected for cFF. For the ^{1}H NMR spectra, NH_2 and NH_2-CH peaks are present in the preheated dipeptide but absent in each aggregate. Furthermore, a COOH peak is obtained in the ^{13}C NMR for the preheated dipeptide but not in any of the aggregates. This pattern matches that which is expected from the molecular structure of *H*-FF-*OH* (NH_2 and COOH present) and cFF (NH_2 and COOH absent). From all this information, it was concluded that each of the white solid aggregates were cFF.

Thus, this characterisation addressed one of the questions of the project, "What is the role of heating solvents in terms of *peptide cyclisation*?"

An investigation carried out by Mason et al. (2014) suggested that the solubility of *H*-FF-*OH* in a solvent depends on the extent of hydrogen bonding between the peptide and the solvent, where a greater solubility correlates to a higher amount of hydrogen bonding.[84] With the chemical structure of the solvents in consideration, it is likely that those which have the electronegative groups -O and –OH, are able to partake in a relatively higher amount of hydrogen bonding than those without. When a peptide is added to such solvents, the solvent O and OH groups interact greatly with the NH_2, NH, CO and OH groups on the peptide. Thus, this is likely the reason of linear *H*-FF-*OH* being relatively insoluble in n-hexane and toluene than the other solvents.

Solvent	Relative polarity*[85]	Boiling point/°C
H_2O	1	100.0
MeOH	0.762	64.7
EtOH	0.654	78.3
n-PrOH	0.617	97.2
i-PrOH	0.546	82.3
THF	0.207	66.0
1,4-Dioxane	0.164	101.0
Toluene	0.099	110.6
n-Hexane	0.009	68.7

*Table 4. The solvents' boiling points and relative polarities. *Values for relative polarity are normalized from measurements of solvent shifts of absorption spectra.*[85]

The following are optical photos and SEM images taken of cFF/H_2O at different magnifications:

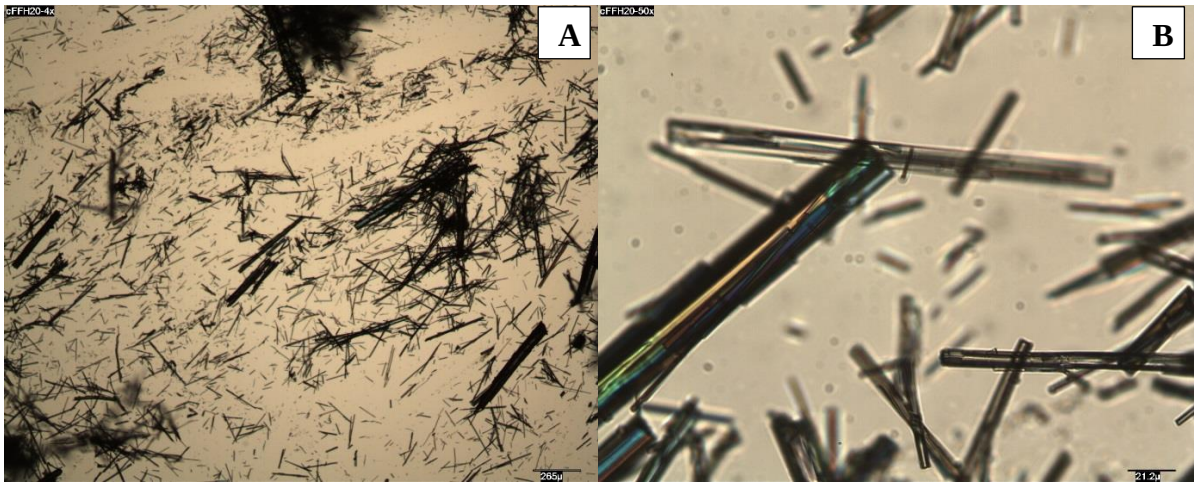

Figure 22. Optical photos of cFF self-assembled in H_2O. (A) is at 4x magnification, with the scale bar in the bottom right at 265 μm. (B) is at 50x magnification, with the scale bar in the bottom right at 21.2μm.

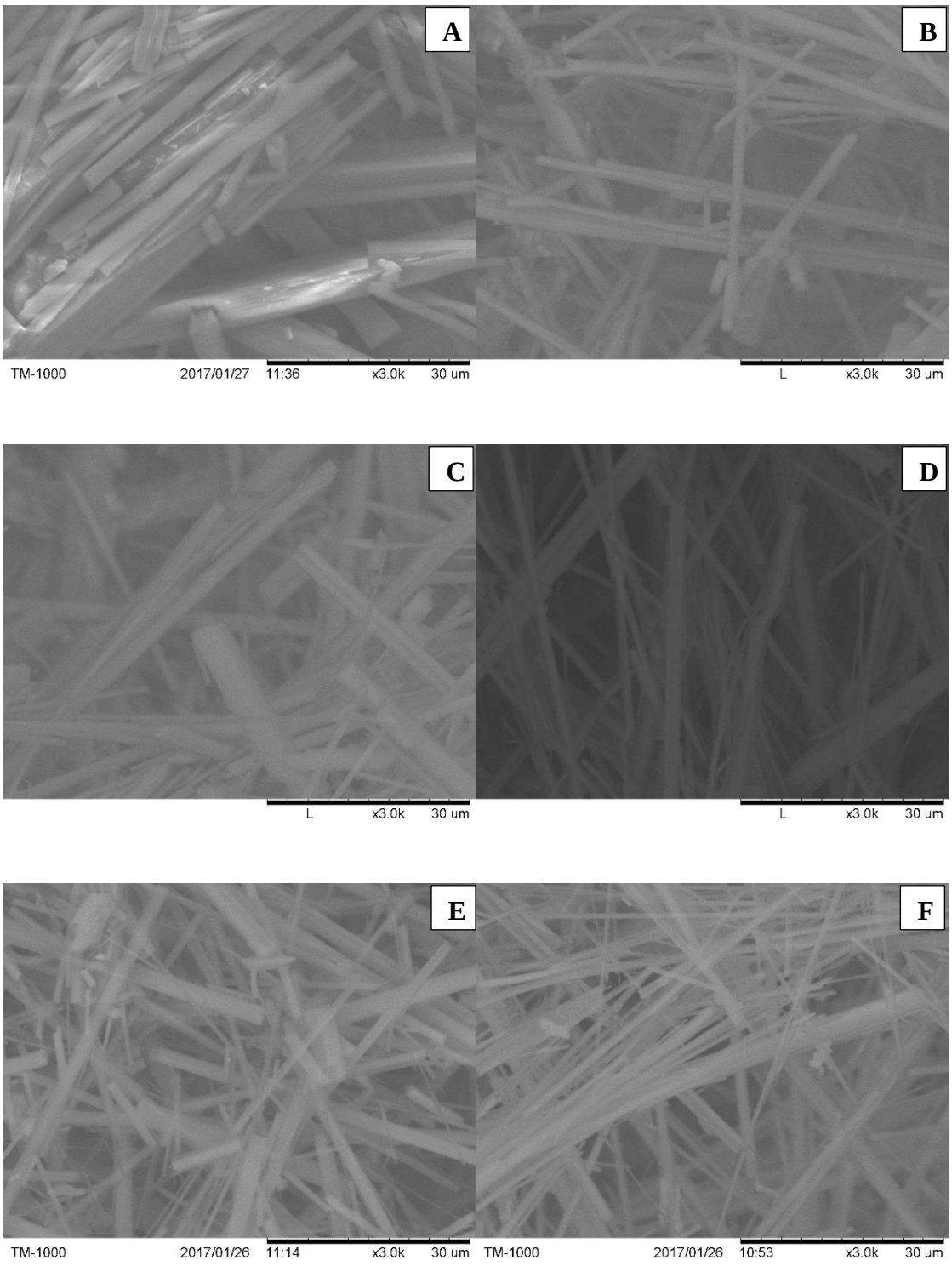

Figure 23. SEM images of cFF obtained from different solvents. (A) H_2O (B) EtOH (C) n-PrOH (D) i-PrOH (E) 1,4-dioxane (F) THF. All images revealed rod-like formations.

From the optical images, it can be seen that the aggregates are made up of individual rod-like strands. In the study performed by Adler-Abramovich et al (2009) in chapter **1**, linear *H*-FF-*OH* was heated to 220 °C, and by the process of vapour deposition, it self-assembled onto a substrate as cyclic FF.[14] The structures were confirmed to be nanotubes, vertically aligned on the substrate.[14] This morphology is very similar to the rods seen in the SEM images (Figs. 23a – f). Even though each sample cyclised and self-assembled in different solvents, the rods from each solvent are nearly identical in appearance.

When the dissolved peptides are heated (and cyclise), the –OH groups in H_2O and the alcohols and the –O groups in the ether analogues (THF and 1,4-dioxane) interact heavily with the functional groups in the cyclic peptide. This cyclic peptide first forms by heating, then subsequently, self-assembly occurs by intermolecular forces between the cyclic peptide-cyclic peptide and cyclic peptide-solvent. In the case of cFF, the phenyl groups favour and participate in aromatic-aromatic interactions, which could contribute to the shape of the rods. Studies have shown that for linear *H*-FF-*OH* in water, hydrogen bonding between the peptide and water drives linear *H*-FF-*OH*'s self-assembly.[2,86] In the similar case of cyclic FF, hydrogen bonding occurs 1) between neighbouring cyclic peptides via the amino and carbonyl groups and 2) between those same groups and the –OH and –O groups from solvent molecules other than water. Additionally, the hydrophobic phenyl groups could also partake in favoured hydrophobic binding.

Hence, the discussion above addressed the second question of the project, "Did the *cyclised peptides* subsequently undergo *self-assembly* in the same solvents they were heated in?"

Heating temperature

For the initial experiments, it was uncertain at which temperatures would be optimal in heating the solutions to yield a self-assembled entity. Therefore, samples of *H*-FF-*OH* were dissolved in each solvent and heated to different temperatures for 12 h. The results can be seen in the following tables (excluding n-hexane and toluene because of *H*-FF-*OH* insolubility). All samples were added to their solvents in a 10 mg/mL concentration.

***H*-FF-*OH* in H_2O**

Temp. for 12h	Physical appearance of sample after heating
30 °C	No change
40 °C	No change
50 °C	Small rod-like strands appear
60 °C	White aggregate
70 °C	White aggregate
80 °C	White aggregate
90 °C	White aggregate

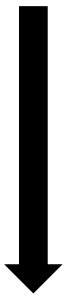

Increasing amount of aggregation

Table 5. Results of heating H-FF-OH in H_2O, 30 °C to 90 °C.

***H*-FF-*OH* in EtOH**

Temp. for 12h	Physical appearance of sample after heating
30 °C	No change
40 °C	No change
50 °C	White aggregate
60 °C	White aggregate
70 °C	White aggregate

Table 6. Results of heating H-FF-OH in EtOH, 30 °C to 70 °C.

***H*-FF-*OH* in n-PrOH**

Temp. for 12h	Physical appearance of sample after heating
30 °C	No change
40 °C	No change
50 °C	White aggregate
60 °C	White aggregate
70 °C	White aggregate
80 °C	White aggregate
90 °C	White aggregate

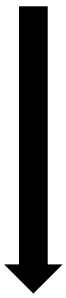

Table 7. Results of heating H-FF-OH in n-PrOH, 30 °C to 90 °C.

***H*-FF-*OH* in i-PrOH**

Temp. for 12h	Physical appearance of sample after heating
30 °C	Small rod-like strands appear
40 °C	White aggregate
50 °C	White aggregate
60 °C	White aggregate
70 °C	White aggregate
80 °C	White aggregate

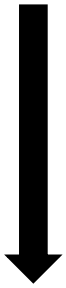

Table 8. Results of heating H-FF-OH in i-PrOH, 30 °C to 80 °C.

***H*-FF-*OH* in 1,4-dioxane**

Temp. for 12h	Physical appearance of sample after heating
30 °C	No change
40 °C	White aggregate
50 °C	White aggregate
60 °C	White aggregate
70 °C	White aggregate
80 °C	White aggregate
90 °C	White aggregate

Table 9. Results of heating H-FF-OH in 1,4-dioxane, 30 °C to 90 °C.

***H*-FF-*OH* in THF**

Temp. for 12h	Physical appearance of sample after heating
30 °C	Small white aggregate
40 °C	White aggregate
50 °C	White aggregate
60 °C	White aggregate

Table 10. Results of heating H-FF-OH in THF, 30 °C to 60 °C.

The minimum temperature was 30 °C, and the highest temperature was 10 °C below the boiling point of each solvent, to avoid the evaporation of the solvent. A general trend can be seen where more self-assembled aggregate is observed at higher temperatures. This could relate to an increased amount of interactions between the molecules. A study which involved the

hydrothermal reactions of a diglycine peptide suggested that the cyclisation of the peptide was more prominent at high temperatures.[87] Another observation is that among the two isomers of propanol, a precipitate can be seen at all temperatures for i-PrOH, whereas for n-PrOH, they can only be seen starting from 50 °C. This could possibly be due to the lower cohesive force of the –OH group in i-PrOH compared to n-PrOH.

It was concluded from these tests that the optimal temperatures would therefore be around 10 °C lower than the boiling point of the solvent, as these temperatures produced visibly more self-assembled aggregate. This temperature rule was applied to the other peptide sequences as well.

Photoluminescence

The group of Lee et al. (2011) undertook research in which cFF nanowires were produced from linear *H*-FF-*OH* via a vapour-transport process.[88] Photoluminescence spectra of these cFF nanowires were taken where an excitation wavelength of 367 nm yielded a relatively strong emission band near 465 nm.[88]

cFF self-assembled in 1,4-dioxane (and filtered) was added to 10 mL of fresh 1,4-dioxane and examined under a spectrofluorometer. An excitation wavelength of 250 nm was used to obtain an emission spectra:

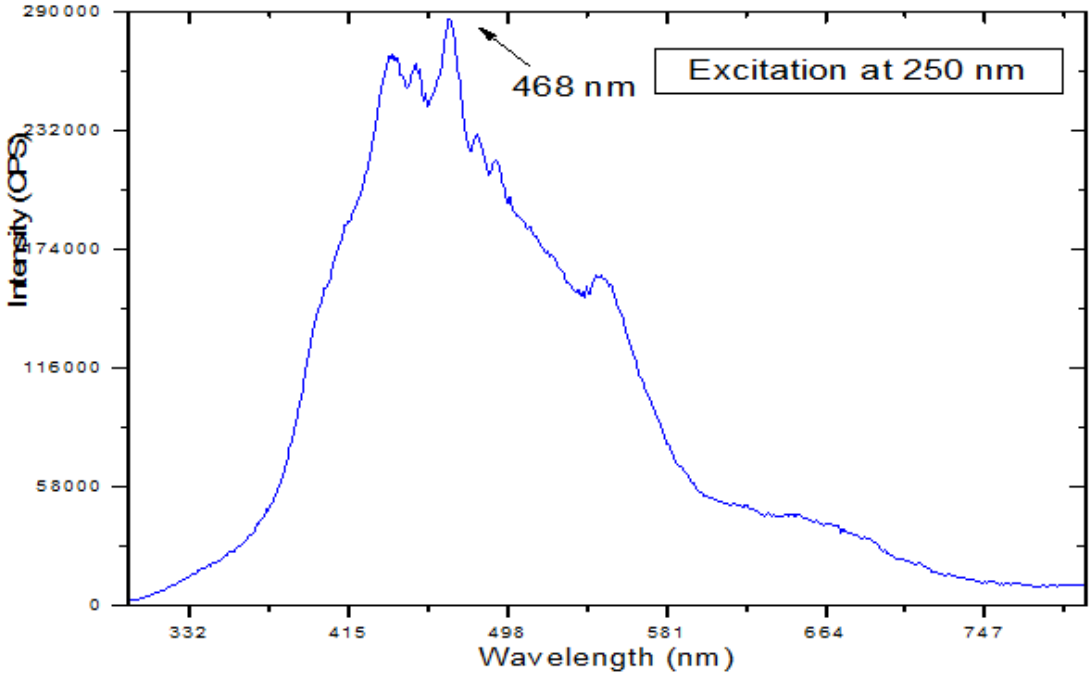

Figure 24. Photoluminescence spectra of cFF/1,4-dioxane, intensity (counts per second) against wavelength (nm). With an excitation at 250 nm, an emission at 468 nm is seen.

Even though the excitation used here was 250 nm, the strong emission at 468 nm is almost the same as the cFF nanowires mentioned earlier. This is the region of blue luminescence. This suggests that cFF self-assembled in different experimental environments could possibly retain its luminescent properties. The strong emission observed here is most likely due to the phenyl rings.[89]

From these experiments, it was concluded that cFF had a preference to form rod-like entities in the different solvents used. This could indicate a specificity in the nature of cFF self-assembly.

3.3 cHH

Unlike diphenylalanine dipeptide, most of the existing literature concerning histidine documents its behaviour when present in long peptide sequences. So far, the self-assembling properties of cyclic dihistidine, specifically, have not been determined. Therefore, there is a great motivation in this case to probe its potential by the method in this project.

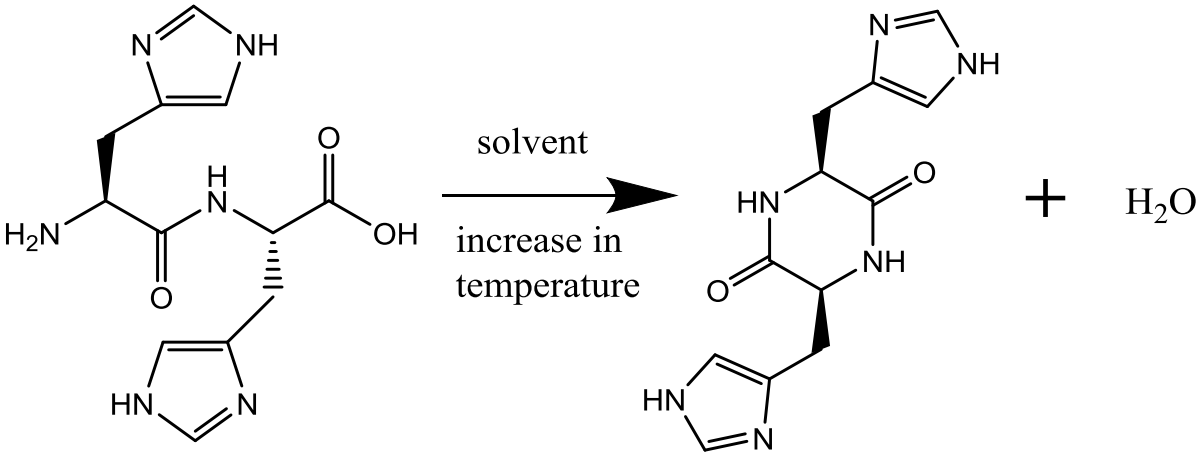

Figure 25. Schematic diagram of H-HH-OH cyclisation.

Depending on the pH, the imidazole group in this dipeptide can be positively charged and the free nitrogen atom can potentially be protonated.

Solvent	Peptide dissolution and solution appearance	Appearance after 12 h heating
H_2O	Insoluble	-
MeOH	Dissolved, colourless	No change
EtOH	Dissolved, colourless	No change
n-PrOH	Dissolved, colourless	Small spherical solid particles in solution
i-PrOH	Insoluble	-
THF	Insoluble	-
1,4-Dioxane	Insoluble	-
Toluene	Insoluble	-
n-Hexane	Insoluble	-

Table 11. Results of H-HH-OH dissolution and appearance after heating.

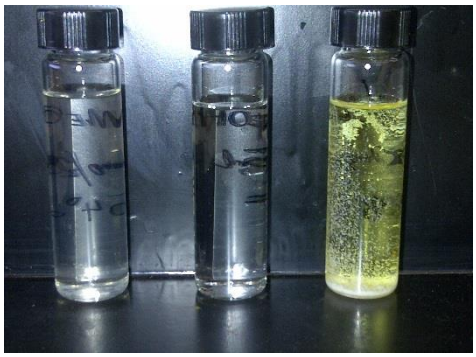

Figure 26. Pictures of sample vials containing dissolved H-HH-OH after heating. From left to right; MeOH, EtOH and i-PrOH. The vials containing MeOH and EtOH had no change but spherical solid particles in a yellow solution were seen for cHH/n-PrOH.

H-HH-*OH* was insoluble in all the non-polar solvents and soluble in the most polar solvents, except for water. *H*-HH-*OH*'s solubility in n-PrOH and insolubility in i-PrOH could be due to n-PrOH being more polar than the latter. Molecular dynamics simulations have shown that in water, a protonated histidine group has a tendency to form like-charged contact pairs with another protonated histidine group.[90] The stability of the resulting *H*-HH-*OH* moiety could be the cause of it not being soluble in water.

The characterisation pattern exhibited for *H*-FF-*OH* and cFF is expected to carry on for the other three dipeptide sequences and their cyclic derivatives. In this case, *H*-HH-*OH* (**2.4.2.**) was compared with the solid particles filtered from n-PrOH (**2.5.7.**). For the mass spectra peaks, the starting dipeptide protonated molecular ion peak was 292.97 $[M + H^+]^+$ whereas that of the solid particles was 274.97 $[M + H^+]^+$. The mass expected for cHH is 274.28 ($[M]^+$). ^{1}H NMR NH_2 and NH_2-CH peaks are observed for *H*-HH-*OH* but not for the solid particles. Likewise, a ^{13}C NMR COOH peak is seen for the starting peptide but not for the solid particles. With this evidence, the solid particles from n-PrOH were confirmed to be cHH.

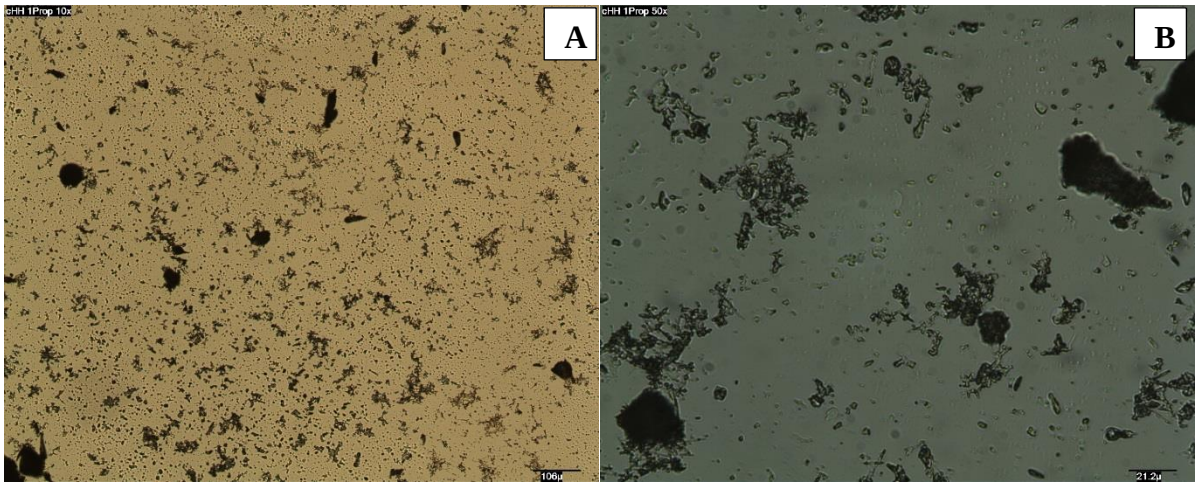

Figure 27. Optical photos of cHH self-assembled in n-PrOH. (A) is at 10x magnification, with the scale bar in the bottom right at 106 µm. (B) is at 50x magnification, with the scale bar in the bottom right at 21.2 µm.

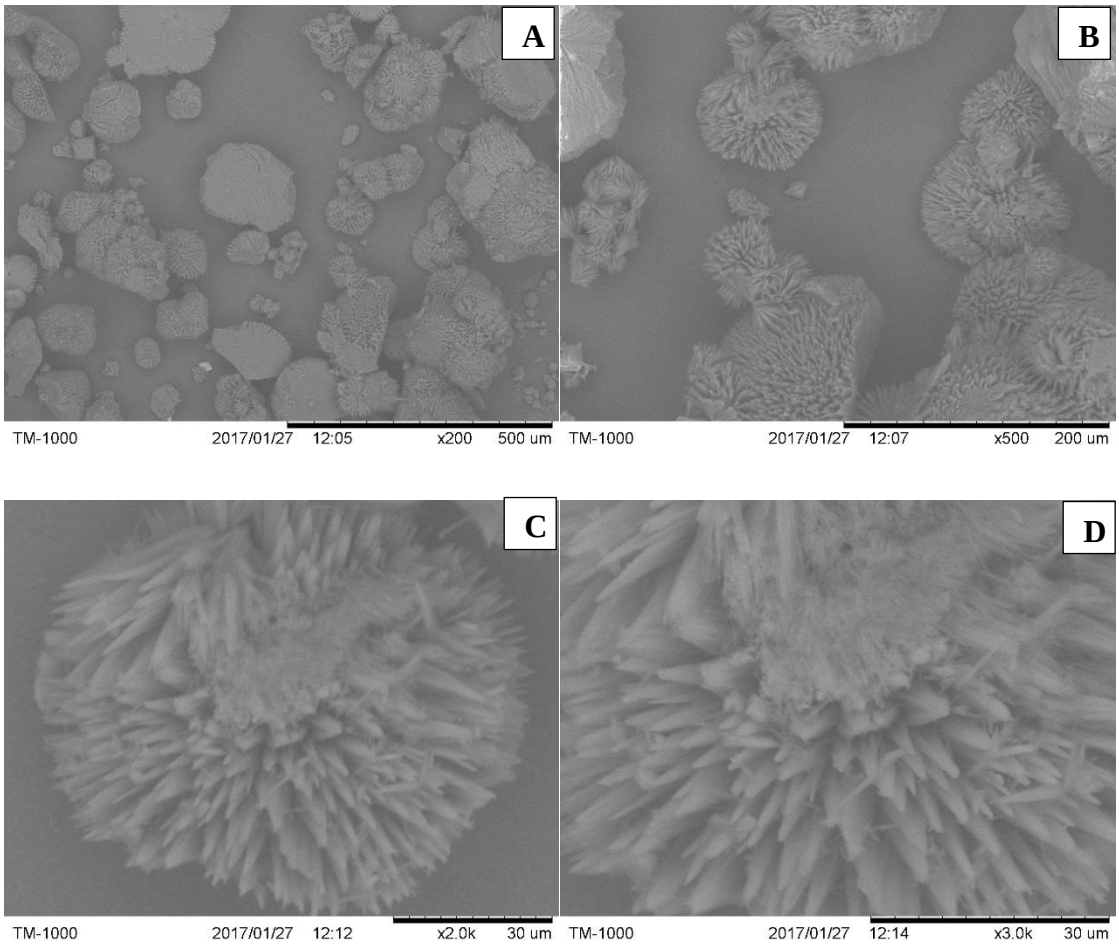

Figure 28. SEM images of cHH obtained from n-PrOH at different magnifications. Higher magnifications (C) and (D) revealed an urchin-like sphere.

From the optical images, the solid particles do not seem to be made of aggregates and are not rod-like like cFF. Looking at the SEM images, many of the solid particles appear to have common spherical features. (Figs. 28a and b). At x2.0k and x3.0k magnifications (Figs. 28c and d), the spheres seem to consist of microneedles outgrowing from a common centre. The spherical formations also appear to be distributed irregularly and not stacked in the same manner as the cFF rods. When comparing the microneedles to the cFF rods at the same magnification (x3.0k; Figs. 28d and figs. 23a – f respectively), a very general observation is that those needle-like structures appear to be smaller than the rods. The arrangement of these structures could be the reason why many of the solid particles are seen sticking to the sample vial's side-wall surfaces. (Fig. 26).

In the three alcohols that *H*-HH-*OH* dissolved in (MeOH, EtOH and n-PrOH), after heating, self-assembly only occurred in n-PrOH. This could be possibly due to the larger chain length of n-PrOH. Like cFF, hydrogen bonding occurs between the cyclic peptide-cyclic peptide and cyclic peptide/solvent, mainly via the -OH group on n-PrOH. In addition to the amino and carbonyl groups on the cyclic peptide, the imidazole ring can participate in aromatic-aromatic stacking. However, this is dependent on the pH of the solvent.[91] Compared to the aromatic-aromatic stacking of cFF's phenyl, the stacking here could possibly be different due to imidazole's different π system. Where phenyl's stacking in cFF produced long regular rods, imidazole's stacking produced needle-like structures that were observably shorter. cHH's self-assembly in n-PrOH produced individual spheroids that aggregated with other spheroids (Figs. 33a and b). Compared to cFF, it is possible that the self-assembly of cHH could be caused by nucleation, giving rise to the observed formations. The spheroid could be described as a hierarchal arrangement similar to what has been called α-Fe_2O_3 (hematite) "urchin-like spheres" by Sun et al. (2012) in their research (even though the centres of those structures were hollow).[92]

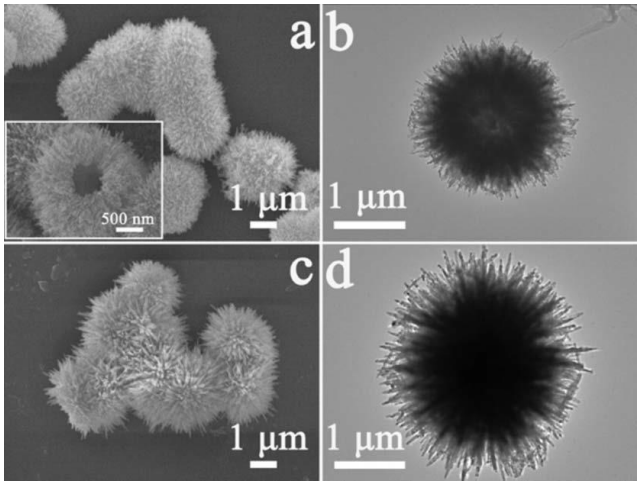

Figure 29. From the work of Sun et al. A hydrothermal process produced FeOOH spheres with hollow structures in water. This was then converted into hollow a-Fe_2O_3 urchin-like spheres via thermal annealing. FESEM (a) and (c) and TEM (b) and (d). (a) and (b) are samples of product synthesised with precursor concentration 0.01 M, (c) and (d) are from precursor concentration 0.1 M.[92]

While the results of cHH/n-PrOH look promising, the lack of self-assembly in the other solvents are unfortunate since the exact cHH self-assembly mechanism could not be probed further using the heating method in this project.

3.4 cHF

Similar to cHH, most of the existing literature only covers histidine coupled with phenylalanine in long peptide sequences and not the dipeptide and/or cyclic dipeptide form. This is also another reason for exploring this dipeptide, and furthermore to see whether, in this sequence, phenylalanine would exhibit its self-assembling tendencies seen in cFF.

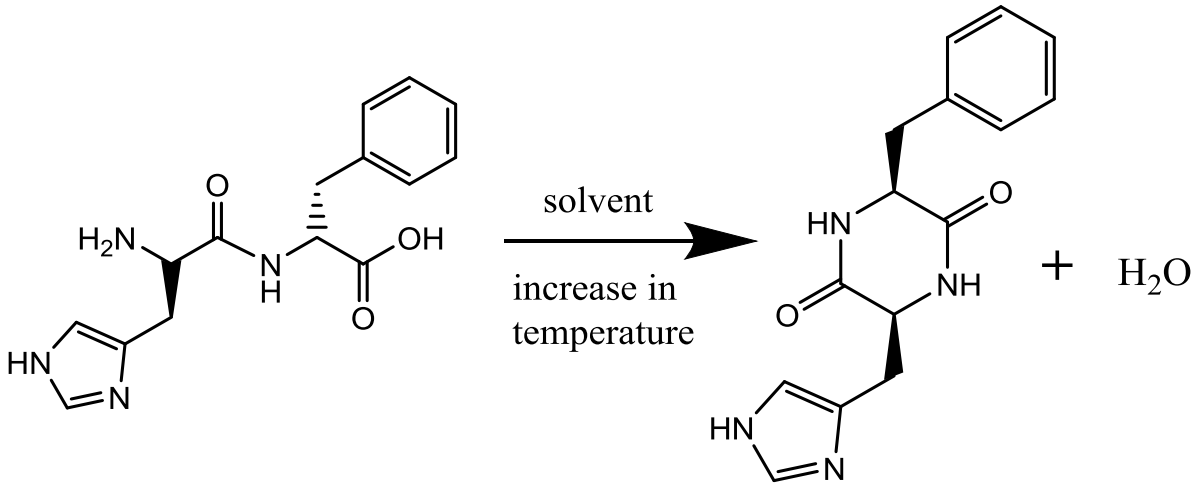

Figure 30. Schematic diagram of H-HF-OH cyclisation.

In this case, both the phenyl and imidazole side chains can influence peptide self-assembly. It is expected that the results would be similar to that of both cFF and cHH.

The solvents used here were the same ones used for the cHH tests; with the exception of EtOH and n-hexane.

Solvent	**Peptide dissolution and solution appearance**	**Appearance after 12 h heating**
H_2O	Dissolved, colourless	No change
MeOH	Dissolved, colourless	No change
n-PrOH	Dissolved, colourless	No change
i-PrOH	Dissolved, colourless	Big urchin-like spherical particles
THF	Dissolved, colourless	Small spherical solid particles in solution
1,4-Dioxane	Insoluble	-
Toluene	Insoluble	-

Table 12. Results of H-HF-OH dissolution and appearance after heating.

Figure 31. Pictures of sample vials containing dissolved H-HF-OH after heating (hence particles are cHF). From left to right; H_2O, MeOH, n-PrOH, i-PrOH and THF. The vials containing H_2O, MeOH and n-PrOH had no change but big solid particles were seen in i-PrOH. Smaller particles were seen in THF.

H-HF-*OH* dissolved in most of the polar solvents, except for 1,4-dioxane, but did not dissolve in the non-polar toluene. The general solubility pattern resembles that of *H*-FF-*OH* more than *H*-HH-*OH*, which suggests that the phenyl ring in *H*-HF-*OH* has more influence in this regard.

With the exception of 1,4-dioxane; compared to *H*-FF-*OH*'s solubility in this solvent, *H*-HF-*OH*'s relative insolubility could be due to the histidine side-chain. In water, since there is only one histidine group in *H*-HF-*OH*, there are no like-charged protonated histidine contact pairs (unlike in *H*-HH-*OH*), and histidine does not form a protonated contact pair with the phenyl group. Therefore, there should be no barriers to *H*-HF-*OH* dissolving in water.

Regarding the characterisation, *H*-HF-*OH* (**2.4.3.**) was compared with the solid particles filtered from both i-PrOH and THF (**2.5.8. - 2.5.9.**). Looking at the mass spectra results, *H*-HF-*OH*'s protonated molecular ion peak was 303.00 $[M + H^+]^+$. One of the solid particles (from i-PrOH) had a protonated molecular ion peak at 285.00 $[M + H^+]^+$ and the other (from THF) at 284.96 $[M + H^+]^+$, where the mass calculated for cHY was 284.32 $([M]^+)$. For the ^{1}H NMR, *H*-HF-*OH* had NH_2 and NH_2-CH peaks whilst neither of the solid particles had them. For the ^{13}C NMR, *H*-HF-*OH* had a COOH peak, but this was not observed in either of the two solid particles. Therefore, both solid particles were cHF.

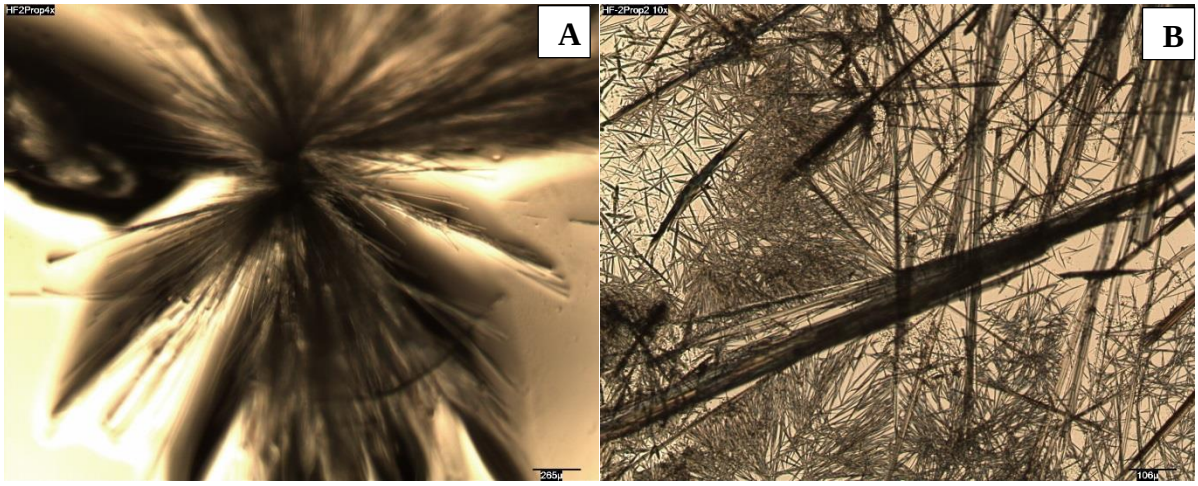

Figure 32. Optical photos of cHF self-assembled in n-PrOH. (A) was taken when cHF was still in the sample vial with the solvent. 4x magnification, with the scale bar in the bottom right at 265 µm. (B) was taken when cHF was filtered from the solvent, where the initial arrangement in (A) broke. 10x magnification, with the scale bar in the bottom right at 106 µm.

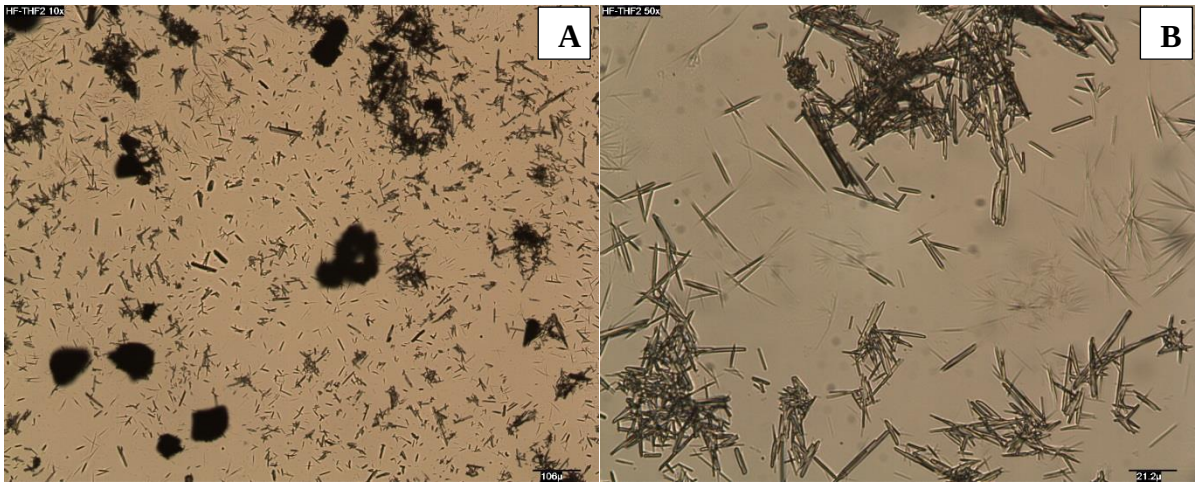

Figure 33. Optical photos of cHF self-assembled in THF. (A) is at 10x magnification, with the scale bar in the bottom right at 106 µm. (B) is at 50x magnification, with the scale bar in the bottom right at 21.2 µm.

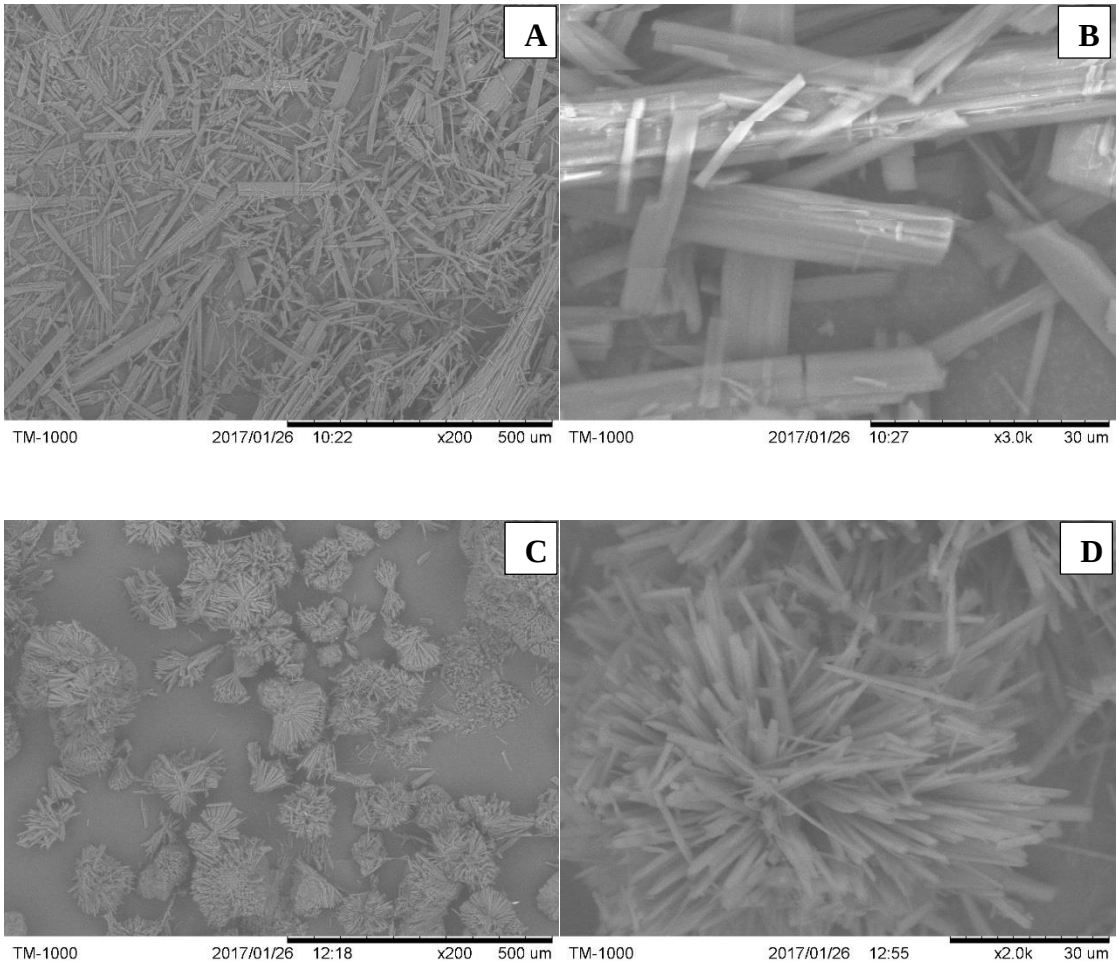

Figure 34. SEM images of cHF self-assembled in different solvents. (A) and (B) are cHF/i-PrOH, which consisted of broken rod-like strands; (C) and (D) are cHF/THF, which mostly consisted of urchin-like spheres.

For cHF self-assembled in i-PrOH, big urchin-like spheres can only be seen when the peptide is in solution (Fig. 32a). However, when it was filtered from the solution, the initial arrangement broke into the rod-like particles seen in Fig. 32b. This can also be seen in the SEM (Figs. 34a and b).

The optical picture of cHF self-assembled in THF at 10x magnification (Fig. 33a) seems to be similar to the same magnification picture of cHH/n-PrOH. However, at 50x magnification, the big solid particles appear to be made up of smaller rods (Fig. 33b).

The SEM images of cHF/i-PrOH (Figs. 34a and b) closely resemble those of cFF, in that individual rod-like strands can be seen. However, compared to the long distinct rods in cFF (for x3.0k magnification, Figs. 28a - f), the cHF rods are shorter in length and are mostly found in bundles. This is likely because these rods were broken from the big urchin-like structures (Figs. 31 and 32a) when they were filtered from the solution. The SEM images of cHF/THF

are more like those of cHH/n-PrOH, where a hierarchal arrangement on this scale can be seen once more. The urchin-like spheroids in Fig. 34c are made up of individual rod-like strands outgrowing from a common centre in Fig. 34d.

In the self-assembly of cHF, apart from the peptide amino and carbonyl functional groups, there will be interactions such as phenyl-solvent, phenyl-phenyl, phenyl-imidazole, imidazole-solvent and imidazole-imidazole. The lack of a self-assembled entity in MeOH is more aligned with the behaviour of cHH, which suggests that the imidazole group might be the reason for this. *H*-HH-*OH* cyclised in and gave a self-assembled formation in n-PrOH, but *H*-HH-*OH* was insoluble in i-PrOH; whereas *H*-HF-*OH* was soluble (and cyclised after heating) in both but gave a self-assembled structure in i-PrOH rather than n-PrOH. cFF self-assembled in both n-PrOH and i-PrOH, so the lack of self-assembly for cHF in n-PrOH is not likely due to the phenyl group alone. It is more likely due to the interactions of both phenyl and imidazole groups and the surface area of OH in i-PrOH compared to n-PrOH. *H*-HH-*OH* was insoluble in THF but *H*-HF-*OH* both dissolved in THF and cHF/THF yielded a self-assembled entity, suggesting that here, the phenyl group had an influence in both dissolution and self-assembly (cFF self-assembled in THF). Looking at both optical and SEM images for cHF/i-PrOH and cHF/THF, the basic building blocks are rod-like and resemble cFF's rods. The reason for this could be due to a significant amount of phenyl-phenyl aromatic-aromatic interactions.

Even though big urchin-like solid spheres were observed for cHF/i-PrOH in solution, these entities broke easily when filtered, leaving behind the rods that formed the sphere. This is in contrast to cHH/n-PrOH, where the spheres were not seen on the optical but rather on the SEM scale, and the urchin-like arrangement was only observed in the SEM images.

When comparing the similar urchin-like formations of cHF and cHH, it is possible that the aromatic-aromatic and hydrogen bonding interactions between the imidazole-imidazole groups is favoured over their interactions with the solvent molecules, causing them to group together. This could be similar to the effect of micelles having their non-polar groups in their centre when they form in solution.[93] In cHF, this tendency to form spheres could also cause a limit on how long the rods could grow out from the centre of each sphere. This could be the reason why the rods seen for cHF/i-PrOH, when broken off, were shorter than the longer ones observed in cFF.

The self-assembly of cHF in THF resembles cHH in n-PrOH more than that of cHF in i-PrOH. In the sense that the urchin-like morphology is mostly seen on the SEM scale and the particles

on the whole are not as big as cHF/i-PrOH. For the most part, the urchin-like formations remain mostly intact after filtration, except for the numerous scattered broken rods seen in the optical (Fig. 33a) and SEM (Fig. 34c) images. Upon closer examination of the SEM (Fig. 34c), cone-like arrangements consisting of rods can be seen, along with two cones joined apex to apex to form a double cone. This is in addition to the full spheres. These cone-like structures could be early stages of self-assembly where cones first form, then are stacked on each other to give a sphere. The individual strands seen in each sphere are rods compared to the needles seen in cHH/n-PrOH, most likely due to the difference in phenyl-phenyl and imidazole-imidazole interactions between the two. The broken rods also indicate that the initial framework can be broken by physical force, however are more stable compared to cHF/i-PrOH where all the spheres easily broke. Concurrently, it is possible that cHF/THF's structural integrity is weaker compared to cHH/n-PrOH, where individual needles could not be seen on the SEM and the spheres remained largely intact.

The self-assembly method of cHF/THF compared to cHF/i-PrOH is likely due to the aprotic nature of THF cf. the protic i-PrOH. The –O in THF is more limited in terms of hydrogen bonding and relies on hydrogens located on the peptide whereas the –OH in i-PrOH has an H available for hydrogen bonding in addition to the oxygen interacting with hydrogens on the peptide.

Both cHF/THF and cHF/i-PrOH conform to the hierarchal organisation seen in cHH/n-PrOH. The grooves in both cHF spheres could cause them to stick to the sample vials (Fig. 31) like cHH/n-PrOH did.

In conclusion, the results for the two solvents are very interesting as they show that the self-assembled formation differs in a different solvent. This breaks the pattern of the previous dipeptides, since cHH only self-assembled in one solvent and cFF had nearly identical formations in each solvent. These results also suggest that the self-assembly for a given dipeptide varies in different solvents (with the conditions used in this project).

3.5 cHY

Even though there is no specific study on the self-assembly of cHY, the self-assembly of tyrosine both by itself and in short peptide sequences has been reported (mentioned in **1.2**).[15,16] Taking the other sequences in this project into account, the results could also shed more light on whether changing a single residue between two dipeptides could affect the overall supramolecular reorganisation (upon heating in the solvents).

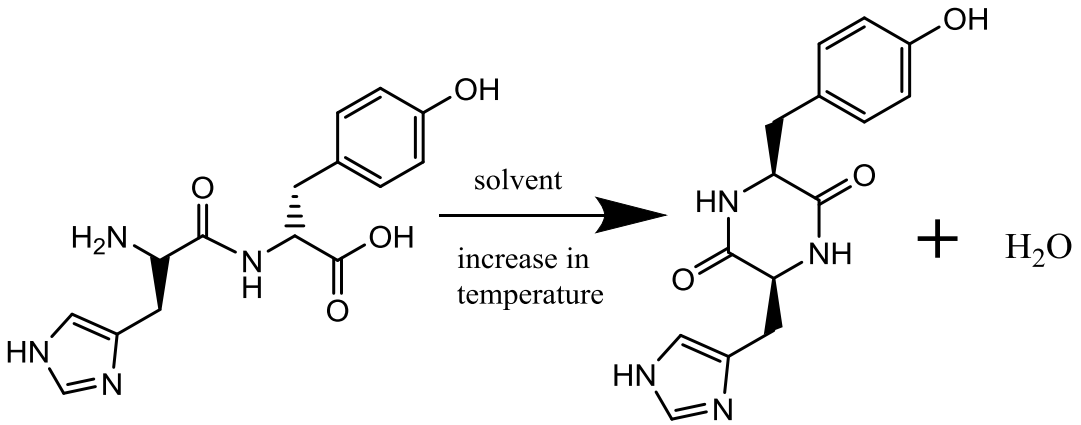

Figure 35. Schematic diagram of H-HY-OH cyclisation.

Here, both the phenol and imidazole side chains can influence peptide self-assembly.

Solvent	**Peptide dissolution and solution appearance**	**Appearance after 12 hours' heating**
H_2O	Dissolved, colourless	No change
MeOH	Dissolved, colourless	No change
n-PrOH	Dissolved, colourless	Yellow solution
i-PrOH	Dissolved, colourless	Solid clumps in solution
THF	Dissolved, colourless	Small spherical solid particles in solution
1,4-Dioxane	Insoluble	-
Toluene	Insoluble	-

Table 13. Results of H-HY-OH dissolution and appearance after heating.

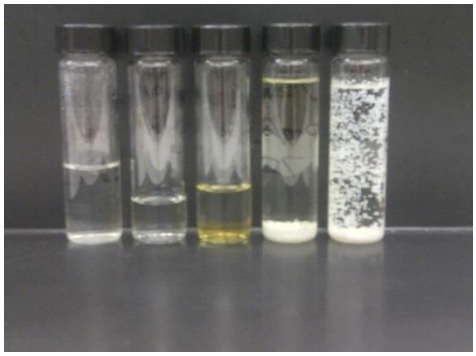

Figure 36. Pictures of sample vials containing dissolved H-HY-OH after heating (hence particles are cHY). From left to right; H_2O, MeOH, n-PrOH, i-PrOH and THF. The vials containing H_2O and MeOH remained unchanged. The vial with n-PrOH had a yellow solution. cHY/i-PrOH gave settled solid particles whereas cHY/THF had scattered solid particles.

H-HY-*OH* was soluble in most of the polar solvents except for 1,4-dioxane, and was insoluble in toluene. Even though, in water, the –OH on the phenol group in Y (tyrosine) could potentially hydrogen bond with the peptide main chain or the imidazole in H (histidine); in this case, any such interactions weren't significant enough to make *H*-HY-*OH* insoluble in water. Apart from the polar –OH group on the phenol (in Y) compared to none on the phenyl (in F), these two side chains are similar in terms of the hydrophobicity of the aromatic ring (in this case, –OH may have a lesser influence versus the aromatic hydrophobicity). From a solubility but not self-assembly perspective, this could explain why *H*-HY-*OH* dissolved in the same solvents *H*-HF-*OH* did.

Characterisation: The starting peptide *H*-HY-*OH* (**2.4.4.**) and the solid particles filtered from both i-PrOH and THF (**2.5.10. - 2.5.11.**) were characterised. The protonated molecular ion peak observed for *H*-HY-*OH*, 319.04 $[M + H^+]^+$, is different than that of particles/i-PrOH, 301.09 $[M + H^+]^+$, and particles/THF, 301.10 $[M + H^+]^+$. The mass calculated for cHY was 300.32 ($[M]^+$). ^{1}H NMR NH_2 and NH_2-CH peaks are seen for *H*-HY-*OH* but not for the solid particles. A ^{13}C NMR COOH peak is seen for the starting peptide but not for the solid particles. Thus, both of the solid particles were determined to be cHY.

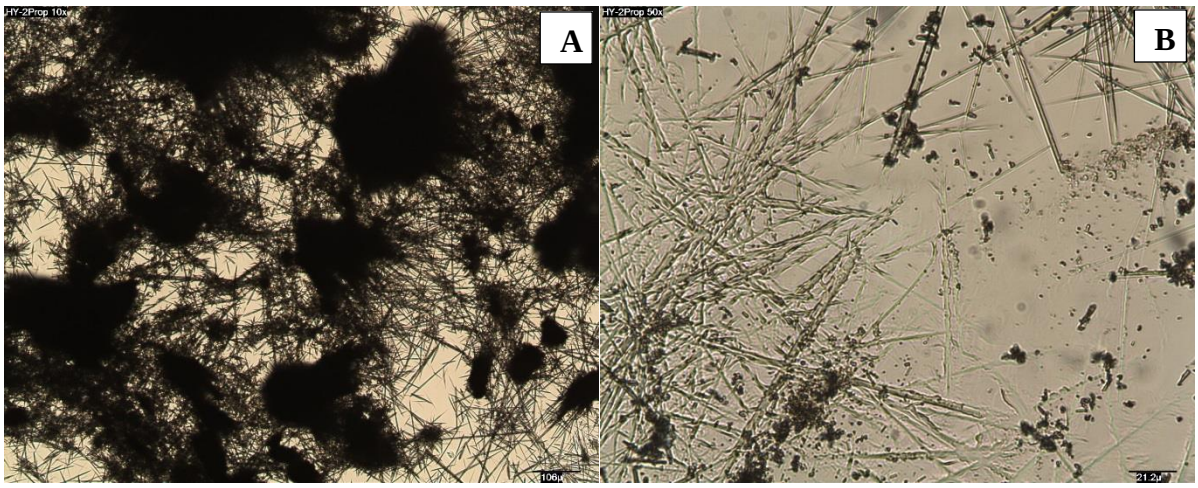

Figure 37. Optical photos of cHY self-assembled in i-PrOH. (A) is at 10x magnification, with the scale bar in the bottom right at 106 µm. (B) is at 50x magnification, with the scale bar in the bottom right at 21.2 µm.

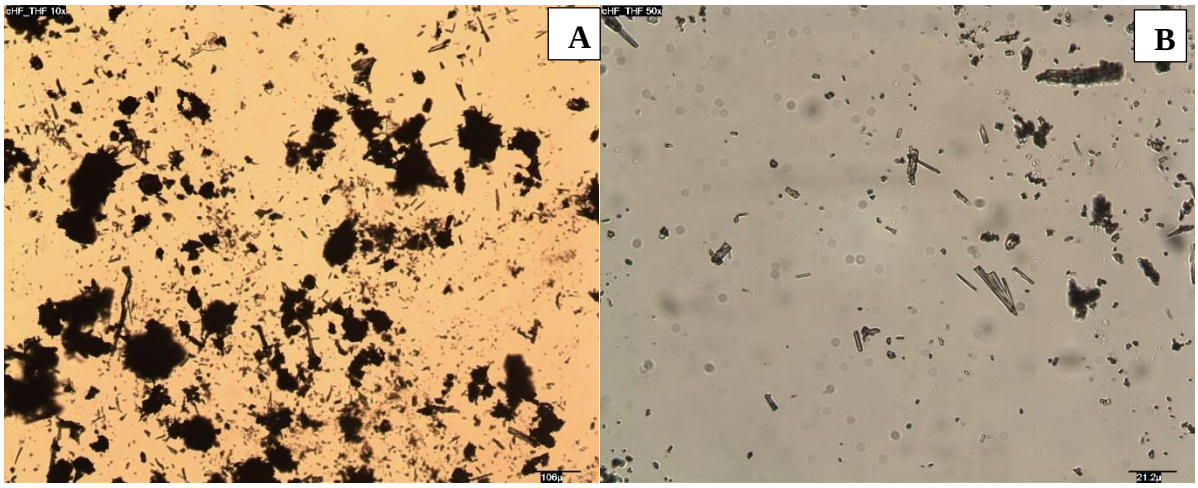

Figure 38. Optical photos of cHY self-assembled in THF. (A) is at 10x magnification, with the scale bar in the bottom right at 106 µm. (B) is at 50x magnification, with the scale bar in the bottom right at 21.2 µm.

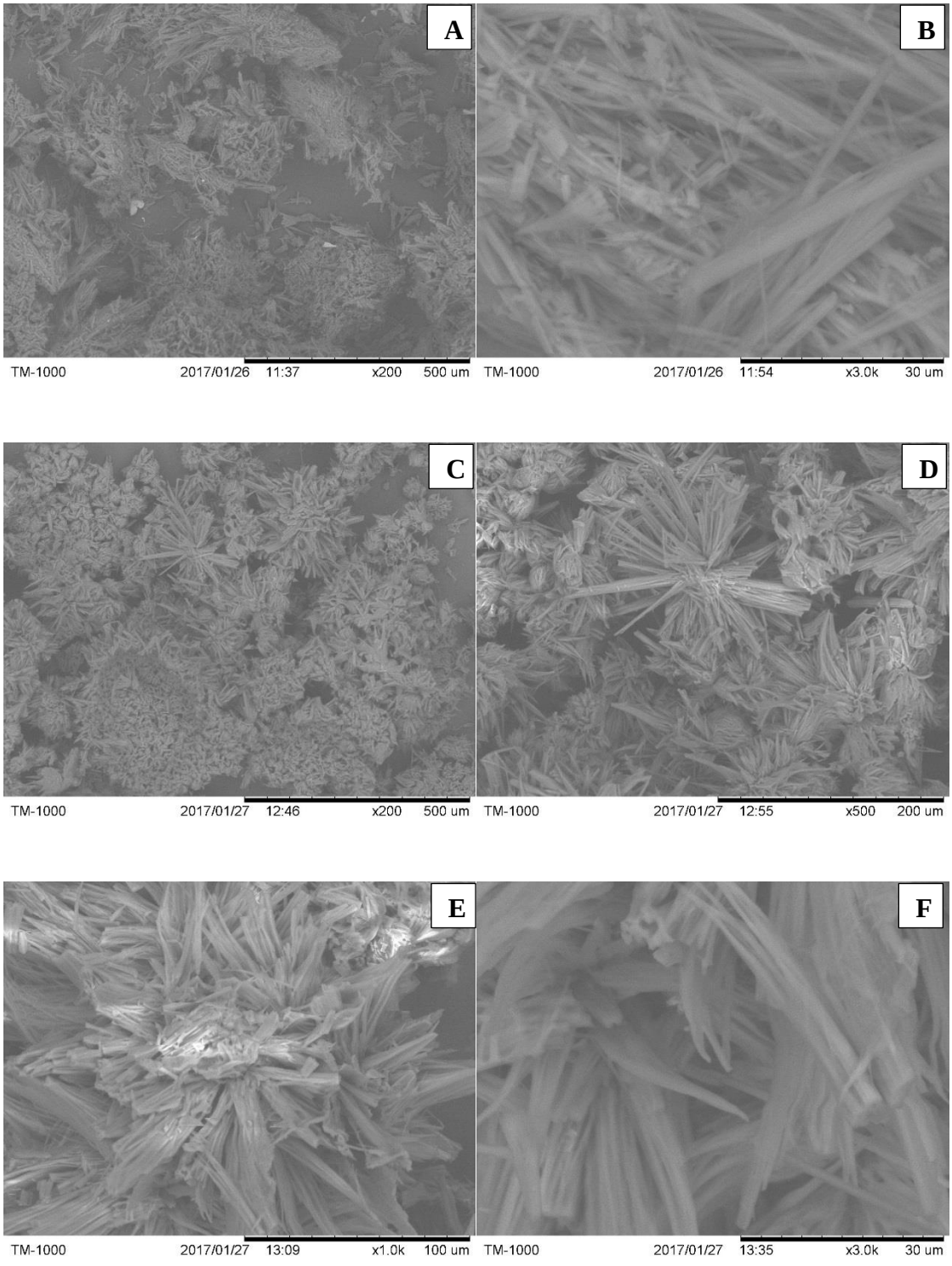

Figure 39. SEM images of cHY self-assembled in different solvents. (A) and (B) are of cHY/i-PrOH, which consisted mostly of rods. (C) – (F) are of cHY/THF at different magnifications. Urchin-like (D) as well as flower-like (E) morphologies can be seen. (F) is a zoom in of the curved rods forming the flower-like.

From the optical, the big solid clumps for cHY/i-PrOH and cHY/THF (Figs. 37a and 38a, resp.) seem to be composed of individual rod-like strands (Figs. 37b and 38b, resp.). However, the individual rod-like strands of cHY/THF (Fig. 38b) appear to be much shorter than those of cHY/i-PrOH (Fig. 37b). It has been demonstrated that in a series of tripeptides of varying terminal amino acid residues, the presence of two terminally positioned Y residues was important in forming nanotubes.[94] The SEM images of cHY self-assembled in i-PrOH break the expected pattern in that urchin-like entities are not seen. Rather, stacks of rod-like strands are observed with no regular distribution (Figs. 39a and b). cHY self-assembled in THF, however, displays the familiar urchin-like organisation (Figs. 39c - f). Although, these formations are not consistent in occurrence and bundles of rods can be seen (Fig. 39c.) The individual cHY rods from both solvents have a similar width to those of cFF. An unusual feature of cHY/THF is that many of the rods are slightly curved (Fig. 39f). This is in contrast to the relatively straight rods seen in cHY/i-PrOH, cHF and cFF. This suggests that these particular rod-like strands may have a degree of flexibility. A consequence of this attribute is that when these strands aggregate into spheres, they produce flower-like structures (Figs. 39d and e). These, along with the urchin-like formations, may be the reason why they stick to the sample vial's walls, whereas cHY/i-PrOH lacks these and settles at the bottom of the vial (Fig. 36).

The self-assembly results are almost identical to that of cHF. The lack of self-assembly in water, MeOH and n-PrOH here also could be due to the imidazole group. It is possible that the coloured solution seen for n-PrOH could be the result of cyclised HF (from heating). However, this mostly remained in the solvent and the intermolecular interactions did not trigger self-assembly and/or precipitation. Which in turn suggests that, in this case, the peptide's bonding with the solvent was more favourable. In terms of molecular forces, Y is similar to F due to the aromatic ring present as phenol. As mentioned in the solubility discussion, the phenol group is different in that the –OH can partake in greater hydrogen bonding. The self-assembly of cHY in i-PrOH yielded individual rod-like strands, much like cFF, possibly due to phenol's aromatic-aromatic stacking. The lack of an urchin-like entity suggests that phenol's stacking and hydrogen bonding are more significant than that of imidazole's. The hydrogen bonding between phenol's –OH and iPrOH's –OH could also be of influence. Even though bundles of rods are seen, they may not be as extensive and ordered as cFF's rods, since those form bigger aggregates to the human eye whilst these (cHY) are relatively small solid clumps. This could be due to differing interactions caused by phenol and imidazole as opposed to the homogeneity

of cFF's two phenyl groups. The bundling in this case (cHY) could be due to van der Waals forces.

For cHY/THF, it appears that imidazole has a significant influence due to the presence of urchin-like formations. This structuring also appears in cHF/THF, which could indicate that the –O ether group in THF is a factor. Since NH-N (imidazole-imidazole) hydrogen bonding is stronger than NH-O[95, 96] (imidazole-THF), the favoured imidazole-imidazole interactions could minimize contact with THF.

Two types of spherical structures are observed. The urchin-like with the straight rods (Fig. 39d) is probably due to phenol's aromatic ring interactions, with lesser input from the –OH group. However, for the flower-like (Figs. 39e and f), in addition to the aromatic stacking, the –OH groups may hydrogen bond significantly with –O in THF, and in a specific direction, giving rise to the curvature of the rods. This curving ability, without the breaking of the strands, could also be due to the inherent flexibility of the rods.

Even after product filtration (from the solvent in the vials), most of the rods seen in cHY/THF were still attached to the bigger spherical aggregates and not broken off (similar to cHF/THF). This suggests a significant amount of intermolecular bonding. In the end, cHY/THF contained a hierarchal entity whereas cHY/i-PrOH did not.

The results recorded for cHY, in addition to the other dipeptides, are interesting because they show that even the change in a single amino acid residue can affect self-assembly. Which in turn confirms the specificity of the nature of self-assembly. However, for this specific dipeptide (cHY), a change between the two solvents did not appear to cause a big variation in the self-assembled formation of the cyclic peptide. This is in clear contrast to cHF.

To summarise, the two main questions set out in this project were answered. The simple heating of predissolved linear dipeptides in different solvents caused cyclisation. All cyclic dipeptides self-assembled in their solvent of origin, with the self-assembly being governed by various intermolecular interactions. Apart from cFF, changing the solvent for a given dipeptide had a visible effect on the self-assembled formation. Lesser to an extent for cHF. Likewise, cyclic dipeptide sequences which varied only by one amino acid residue (cFF cf. cHF; cHF cf. cHY), for a given solvent, also displayed a change in their self-assembled formations.

Chapter Four

Conclusions

Chapter 4. Conclusions and future work

This project aimed to determine the self-assembly of dipeptides after they cyclised in different solvents upon heating.

Four dipeptides, *H*-FF-*OH*, *H*-HH-*OH*, *H*-HF-*OH* and *H*-HY-*OH* were successfully synthesised by Fmoc SPPS with a Wang resin. The testing of each peptide in the solvents yielded the following results.

H-FF-*OH* was soluble in all of the polar solvents used, and cyclised in each solvent. White solid-like aggregates were seen by the human eye, and optical and SEM images revealed consistent rod-like frameworks. The self-assembly in this case was caused by the aromatic-aromatic stacking of cFF's phenyl group, possibly its hydrophobic binding, and hydrogen bonding throughout the peptide. cFF cyclised in 1,4-dioxane also exhibited blue luminescent properties. Temperature tests showed that the higher the temperature, the greater the amount of solid aggregation (by human eye). With this result, it was concluded that the best temperature for heating all four dipeptides would be 10 °C lower than the respective solvent's boiling point.

H-HH-*OH* dissolved in the more polar solvents except for water. This could be due to a protonated histidine group forming a like-charged contact pair with another protonated histidine group, making the *H*-HH-*OH* moiety much more stable in water. cHH only exhibited self-assembly in n-PrOH, possibly due to n-PrOH's chain length, and displayed a hierarchal entity. Urchin-like spheres were seen which seemed to be made up of smaller needles aggregated together. The cause of this arrangement could be due to the specific aromatic-aromatic interactions of histidine's imidazole.

H-HF-*OH* dissolved in the more polar solvents, resembling *H*-FF-*OH*'s solubility. Its insolubility in 1,4-dioxane could be due to the histidine group. cHF self-assembled in i-PrOH and THF. To the human eye, cHF/i-PrOH had a big urchin-like appearance whereas cHF/THF was seen as small spherical particles. After each compound was filtered from its solvent, images showed cHF/i-PrOH to be made of rods which were broken off from the bigger particles seen in the sample vial. cHF/THF retained its hierarchal arrangement, similar to cHH/n-PrOH, and appeared to be made of smaller rods aggregating to give an urchin-like formation. The self-assembly of cHF in i-PrOH could have initially given a stable entity in the solvent, but the

molecular forces were not strong enough to hold the initial structure when it was filtered. The self-assembly of cHF in THF could have been stronger because of cHF's interactions with the THF –O group, and the urchin-like structure could be the result of histidine's imidazole groups.

H-HY-*OH* dissolved in the same solvents that *H*-HF-*OH* did, which could be due to the similarity between Y's phenol and F's phenyl. cHY self-assembled in i-PrOH and THF. cHY/i-PrOH did not appear to have a hierarchal structure but instead seemed to be made of bundles of rods. This similarity to cFF's rods could be due to Y's phenol's aromatic-aromatic stacking. cHY/THF had two types of hierarchal entities. The urchin-like with the straight rods was probably a result of phenol's aromatic ring interactions. The flower-like was likely due to both cHY's aromatic stacking and significant hydrogen bonding with THF's –O. The specific directionality of this bonding could also have caused the rods to curve.

For future work, the exact crystallography of each self-assembled cyclised peptide could also be elucidated by techniques such as powder X-ray diffraction, FESEM, AFM and TEM. An investigation into peptide gelation in a range of other solvents should also be undertaken. Physical properties of the self-assembled products could be tested, such as photoluminescence, rheology, electrical and fluorescence. The kinetics of heating each peptide in their solvent should also be probed. By the same heating method, other dipeptide sequences such as *H*-FW-*OH* and *H*-YW-*OH* should also be experimented on. Regarding the histidine-based dipeptides, their self-assembly could be tested via binding to metals such as Cu^{2+}.

References

1. Y. Loo, S. Zhang and C. A. E. Hauser, *Biotechnol. Adv.*, 2012, **30**, 593–603.

2. C. H. Görbitz, *Chem. Commun.*, 2006, **22,** 2332-2334.

3. E. Gazit, *Chem. Soc. Rev.*, 2007, **36**, 1263-1269.

4. K. E. Schwiebert, D. N. Chin, J. C. MacDonald and G. M. Whitesides, *J. Am. Chem. Soc.*, 1996, **118**, 4018–4029.

5. C. De Rosa, C. Park, E. L. Thomas and B. Lotz, *Nature*, 2000, **405**, 433-437.

6. Y. Huang, P. G. Lawrence and Y. Lapitsky, *Langmuir*, 2014, **30**, 7771–7777.

7. D. Philp and J.F. Stoddart, *Angew. Chem. Int. Ed.*, 1996, **35**, 1154–1196.

8. G. M. Whitesides and M. Boncheva, *Proc. Natl. Acad. Sci. U.S.A.*, 2002, **99**, 4769–4774.

9. M. Monthioux and V. L. Kuznetsov, *Carbon*, 2006, **44**, 1621-1623.

10. M. R. Ghadiri, J. R. Granja, R. A. Milligan, D. E. McRee and N. Khazanovich, *Nature*, 1993, **366**, 324 – 327.

11. S. Zhang, *Nat. Biotechnol.*, 2003, **21**, 1171-1178.

12. L. Adler-Abramovich and E. Gazit, *Chem. Soc. Rev.*, 2014, **43**, 6881—6893.

13. X. Yan, Y. Cui, Q. He, K. Wang and J. Li, *Chem. Mater.* 2008, **20**, 1522–1526.

14. L. Adler-Abramovich, D. Aronov, P. Beker, M. Yevnin, S. Stempler, L. Buzhansky, G. Rosenman and E. Gazit, *Nat. Nanotechnol.*, 2009, **4**, 849-854.

15. C. Ménard-Moyon 1, V. Venkatesh, K. V. Krishna, F. Bonachera, S. Verma and A. Bianco, *Chem. Eur. J.*, 2015, **21**, 11681 – 11686.

16. K.I. Min, G. Yun, Y. Jang, K. R. Kim, Y. H. Ko, H. S. Jang, Y. S. Lee, K. Kim and D. P. Kim, *Angew. Chem. Int. Ed.* 2016, **55**, 6925 –6928.

17. H. Sigel and D. B. McCormick, *J. Am. Chem. Soc.*, 1971, **93**, 2041–2044.

18. F. Aldeek, M. Safi, N. Zhan, G. Palui and H. Mattoussi, *ACS Nano*, 2013, **7**, 10197–10210.

19. A. Jeziorna, K. Stopczyk, E. Skorupska, K. Luberda-Durnas, M. Oszajca, W. Lasocha, M. Górecki, J. Frelek and M. J. Potrzebowski, *Cryst. Growth Des.*, 2015, **15**, 5138–5148.

20. A. J. Kleinsmann and B. J. Nachtsheim, *Chem. Commun.*, 2013, **49**, 7818-7820.

21. I. M. Atkinson, L. F. Lindoy and J. F. Stoddart, *Self Assembly in Supramolecular Systems: RSC (Monographs in Supramolecular Chemistry)***,** Royal Society of Chemistry, Cambridge, 2000.

22. K. C. B. Chandra and F.D'Souza, *Coord. Chem. Rev.*, 2016, **322**, 104–141.

23. G. M. Whitesides and M. Boncheva, *Proc. Natl. Acad. Sci. U.S.A.*, 2002, **99**, 4769–4774.

24. J. W. Steed and J. L. Atwood, *Supramolecular* Chemistry, Wiley-Blackwell, Hoboken, New Jersey, 2009.

25. G. M. Whitesides, J. K. Kriebel and B. T. Mayers, in *Nanoscale Assembly: Chemical Techniques*, ed. W. T. S. Huck, Springer US, New York, 1st edn, 2005, ch. 9, pp. 217-239.

26. K. Hanabusa and M. Suzuki, *Polym. J.*, 2014, **46**, 776-782.

27. G. B. McGaughey, M. Gagné and A. K. Rappé, *J. Biol. Chem.*, 1998, **273**, 15458-63.

28. S.Grimme, *Angew. Chem. Int. Ed.*, 2008, **47**, 3430 –3434.

29. C. R. Martinez and B. L. Iverson, *Chem. Sci.*, 2012, **3**, 2191–2201.

30. P. R. Ashton, M. C. T. Fyfe , P. T. Glink, S. Menzer, J. F. Stoddart, A. J. P. White and D. J. Williams, *J. Am. Chem. Soc.*, 1997, **119**, 12514–12524.

31. V. Balzani, M. Gómez-López and J. F. Stoddart, *Acc. Chem. Res.* 1998, **31**, 405-414.

32. D. A. Dougherty, *J. Nutr.*, 2007, **137**, 1504S-1508S.

33. H. S. Frank and M. W. Evans, *J. Chem. Phys.*, 1945, **13**, 507–532.

34. D. Laage, G. Stirnemann, F. Sterpone, R. Rossend and J. T. Hynes, *Annu. Rev. Phys. Chem.*, 2011, **62**, 395–416.

35. R. L. Baldwin, *Proc. Natl. Acad. Sci. U.S.A.*, 2014, **111**, 13052–13056.

36. C. Eicken, V. Sharma, T. Klabunde, M. B. Lawrenz, J. M. Hardham, S. J. Norris and J. C. Sacchettini, *J. Biol. Chem.*, 2002, **277**, 21691-6.

37. C. N. Pace, H, Fu, K. L. Fryar, J. Landua, S. R. Trevino, B. A. Shirley, M. M. Hendricks, S. Iimura, K. Gajiwala, J. M. Scholtz, G. R. Grimsley, *J Mol Biol.*, 2011, **408**, 514-28.

38. L. Stryer, *Stryer's Biochemistry, Fourth Edition*, W. H. Freeman and Company, New York, 1998.

39. Y. Gnanou and M. Fontanille, *Organic and Physical Chemistry of Polymers*, John Wiley & Sons, Hoboken, New Jersey, 2008.

40. P. A. Kollman, *Acc. Chem. Res.*, 1977, **10**, 365–371.

41. C. Liébecq, *Biochemical Nomenclature & Related Documents: A Compendium*, Portland Press, London, 1992.

42. D. J. Adams, *Macromol. Biosci.*, 2011, **11**, 160-73.

43. CyBase, http://www.cybase.org.au/, (accessed February 2017).

44. Huan-X. Zhou, *Acc. Chem. Res.*, 2004, **37**, 123–130.

45. M. Katsara, T. Tselios, S. Deraos, G. Deraos, M. T. Matsoukas, E. Lazoura, J. Matsoukas and V. Apostolopoulos, *Curr. Med. Chem.*, 2006, **13**, 2221-32.

46. G. L. Amidon, H. J. Lee, *Annu. Rev. Pharmacol. Toxicol.*, 1994, **34**, 321-41.

47. L. Pérez-Picaso, J. Escalante, H. F. Olivo and M. Y. Rios, *Molecules*, 2009, **14**, 2836-2849.

48. A. D. Borthwick, *Chem. Rev.*, 2012, **112**, 3641–3716.

49. C. Cornacchia, I. Cacciatore, L. Baldassarre, A. Mollica, F. Feliciani and F. Pinnen, *Mini Rev Med Chem.*, 2012, **12**, 2-12.

50. M. A. Abdalla, *Nat. Prod. Res.*, 2017, **31**, 1014–1021.

51. Y. Mohammed, M. Teixidó, S. Namjoshi, E. Giralt and H. Benson, *PLoS One*, 2016, DOI:10.1371/journal.pone.0160973.

52. S. Manchineellaa and T. Govindaraju, *RSC Adv.*, 2012, **2**, 5539-5542.

53. J. S. Davies, *J. Peptide Sci.*, 2003, **9**, 471–501.

54. Y. Zhu, M. Tang, X. Shi and Y. Zhao, *Int. J. Quantum Chem.*, 2007, **107**, 745-753.

55. C. J. Balibar and C. T. Walsh, *Biochemistry*, 2006, **45**, 15029-15038.

56. Y. Qian, M. H. Engel, S. A. Macko, S. Carpenter and J. W. Deming, *Geochim. Cosmochim. Acta*, 1993, **57**, 3281-3293.

57. N. E. Leadbeater, *Microwave Heating as a Tool for Sustainable Chemistry (Sustainability: Contributions Through Science and Technology)*, CRC Press, Boca Raton, Florida, 2010.

58. D. P. Barondeau, C. D. Putnam, C. J. Kassmann, J. A. Tainer and E. D. Getzoff, *Proc. Natl. Acad. Sci. U.S.A.*, 2003, **100**, 12111–12116.

59. F.W. Lichtenthaler, *Eur. J. Org. Chem.*, 2002, **2002**, 4095–4122.

60. E. Fischer and E. Fourneau, *Ber. Dtsch. Chem. Ges.*, 1901, **34**, 2868–2877.

61. S. Chandrudu, P. Simerska and I. Toth, *Molecules.*, 2013, **18**, 4373-88.

62. L. A. Carpino, S. Ghassemi, D. Ionescu, M. Ismail, D. Sadat-Aalaee, G. A. Truran, E. M. E. Mansour, G. A. Siwruk, J. S. Eynon and B. Morgan, *Org. Proc. Res. Dev.*, 2003, **7**, 28–37.

63. J. Wu, G. An, S. Lin, J. Xie, W. Zhou, H. Sun, Y. Pana and G. Li, *Chem. Commun.*, 2014, **50**, 1259-1261.

64. A. B. Hughes, *Building Blocks, Catalysis and Coupling Chemistry: Volume 3 (Amino Acids, Peptides and Proteins in Organic Chemistry (VCH))*, Wiley VCH, Weinheim, 2010.

65. R. B. Merrifield, *J. Am. Chem. Soc.*, 1963, **85**, 2149–2154.

66. J. Lenard and A. B. Robinson, *J. Am. Chem. Soc.*, 1967, **89**, 181-2.

67. M. Stawikowski and G. B. Fields, Introduction to Peptide Synthesis, *Curr. Protoc. Protein Sci*., 2002, Unit 18.1.

68. R. B. Merrifield, *Science*, 1986, **232**, 341-7.

69. T. J. Lukas, M. B. Prystowsky and B. W. Erickson, *Proc. Nati. Acad. Sci. U.S.A.*, 1981, **78**, 2791-2795.

70. E. Atherton, M. J. Gait, R. C. Sheppard and B. J. Williams, *Bioorg. Chem.*, **8**, 1979, 351-370.

71. R. Behrendt, P. White and J. Offer, *J. Pept. Sci.*, 2016, **22**, 4–27.

72. S. B. Kent, A. R. Mitchell, M. Engelhard and R. B. Merrifield, *Proc Natl. Acad. Sci. U.S.A.*, 1979, **76**, 2180-4.

73. E. Atherton and R. C. Sheppard, *Solid Phase Peptide Synthesis: A Practical Approach*, Oxford University Press, Oxford, 1989.

74. L. A. Carpino and G. Y. Han, *J. Org. Chem.*, 1972, **37**, 3404–3409.

75. W. C. Chan and P. D. White, *Fmoc Solid Phase Peptide Synthesis: A Practical Approach*, Oxford University Press, Oxford, 2000.

76. G. Walter, *J. Immunol. Methods*, 1986, **88**, 149-61.

77. H. Acar, PhD thesis, Bilkent University, 2012.

78. N. Na, X. Mu, Q. Liu, J. Wen, F. Wang and J. Ouyang, *Chem. Commun.*, 2013, **49**, 10076-10078.

79. M. Jaworska, A. Jeziorna, E. Drabik and M. J. Potrzebowski, *J. Phys. Chem. C*, 2012, **116**, 12330−12338.

80. T. Togashi, M. Umetsu, H. Tsuchizaki, S. Ohara, T. Naka and T. Adschiri, *Chem. Lett.*, 2006, **35**, 636-637.

81. A. Handelman, N. Kuritz, A. Natan and G. Rosenman, *Langmuir*, 2016, **32**, 2847−2862.

82. C. Bérubé, X. Barbeau, S. Cardinal, P. Boudreault, C. Bouchard, N. Delcey, P. Lagüe and N. Voyer, *Supramol. Chem.*, 2017, **29**, 330–349.

83. W. R. Jackson, G. S. Jayatilake, B. R. Matthews and C. Wilshire. *Aust. J. Chem.*, 1988, **41**, 203-13.

84. T. O. Mason, D. Y. Chirgadze, A. Levin, L. Adler-Abramovich, E. Gazit, T. P. J. Knowles and A. K. Buell, *ACS Nano*, 2014, **8**, 1243-1253.

85. C. Reichardt and T. Welton, *Solvents and Solvent Effects in Organic Chemistry*, John Wiley & Sons, Hoboken, New Jersey, 2010.

86. C. H. Görbitz, *Chem Eur J.*, 2001, **7**, 5153–5159.

87. J. Li and T. B. Brill, *J. Phys. Chem. A*, 2003, **107**, 8575–8577.

88. J. S. Lee, I. Yoon, J. Kim, H. Ihee, B. Kim and C. B. Park, *Angew. Chem. Int. Ed.*, 2011, **50**, 1164 –1167

89. G. M. Barenboĭm, A. N. Domanskiĭ, K. K. Turoverov, *Luminescence of Biopolymers and Cells*, Springer, New York City, 1969.

90. J. Heyda, P. E. Mason and P. Jungwirth, *J. Phys. Chem. B*, **114**, 2010, 8744–8749.

91. R. H. Blessing and E. L. McGandy, *J. Am. Chem. Soc.*, **94**, 1972, 4034–4035.

92. P. Sun, Z. Zhu, P. Zhao, X. Liang, Y. Sun, F. Liua and G. Lu, *CrystEngComm*, 2012, **14**, 8335-8337.

93. A. Nikoubashmana, *Soft Matter*, 2017, **13**, 222-229.

94. S. Ray, M. G. B. Drew, A. K. Das and A. Banerjee, *Tetrahedron*, 2006, **62**, 7274–7283.

95. J. W. Larson and T. B. McMahon, *Inorg. Chem.*, 1984, **23**, 2029–2033.

96. J. Emsley, *Chem. Soc. Rev.*, 1980, **9**, 91-124.